POLITECNICO DI TORINO

Corso di Laurea in Ingegneria Biomedica

Tesi di Laurea Magistrale

Neurostimulation with Electromagnetic Waves in the Millimetre Range

POLITECNICO
DI TORINO

Relatori
prof. Danilo Demarchi
dr. Timothy Constandinou

Luigi Belcastro
matricola: 220979

Marzo 2018

Contents

List of Figures V

Abbreviations and symbols VII

Summary IX

1 Introduction 1
- 1.1 Electromagnetic waves . . . 3
- 1.2 Frequency behaviour of dielectrics . . . 7
- 1.3 Millimetre waves in Therapy . . . 9
- 1.4 Bio-heat transfer . . . 10
- 1.5 Nervous System . . . 11
- 1.6 Neural Stimulation . . . 15
- 1.7 Objective . . . 17
- 1.8 Materials and methods . . . 17

2 Nerve Model 19
- 2.1 Gabriel model . . . 19
- 2.2 Anatomical Model . . . 21
- 2.3 2D models and mesh . . . 23
- 2.4 Materials . . . 26
- 2.5 Step 1: EM waves, frequency domain . . . 28
- 2.6 Step 2: Bio-heat transfer . . . 30

3 Results 33
- 3.1 Reference value and setup . . . 33
- 3.2 Gabriel model vs anatomic model . . . 34
- 3.3 Superficial vs deep focusing . . . 35
- 3.4 Optimal number of active sources . . . 37
- 3.5 Dielectric spacer thickness . . . 41
- 3.6 Extended time . . . 41
- 3.7 Increase in power . . . 42

4 Discussion 51
4.1 Future work 52

Bibliography 55

List of Figures

1.1 Lossy dielectric (1.1a) and circuit equivalent (1.1b) 7
1.2 Polarization inside a dielectric. 8
1.3 Parasympathetic nervous system. 12
1.4 Nerve anatomy. 13
1.5 Membrane voltage during an action potential. 14
1.6 Concept of the hypothetical device. 18

2.1 Frequency dependence of dielectric properties of the nervous tissue in the range 10 - 200GHz 20
2.2 Comparison of relative permittivity (2.2a) and conductivity (2.2b) of tissues and models of epineurium and endoneurium in the frequency range 10 - 200GHz. 24
2.3 Comparison between the relative permittivity and conductivity of the two connective tissues. 25
2.4 Cross section of a human sural nerve and 3D model of the nerve. . 25
2.5 Geometry of the model. 26
2.6 Mesh detail. 27
2.7 Port boundary condition. 29
2.8 Relationship between SAR and exposure time to obtain a ΔT of 1°C. 31

3.1 Numbering of the fascicles. 33
3.2 Comparison of SAR and ΔT between the anatomic model and the Gabriel model (superficial focusing). 36
3.3 Comparison of SAR and ΔT between the anatomic model and the Gabriel model (deep focusing). 37
3.4 Bar plot of average SAR inside the 12 fascicles. 38
3.5 Bar plot of average ΔT inside the 12 fascicles. 39
3.6 Color map of the SAR for deep and superficial focusing at three frequencies. 40
3.7 Color map of the ΔT for deep and superficial focusing at three frequencies. 44
3.8 Ideal number of active source for focusing at three frequencies. . . 45

3.9 Ideal width of dielectric spacer for power transfer at three frequencies. 46
3.10 Evolution of ΔT in time for 100ms. 47
3.11 Evolution of ΔT in time for 10s. 47
3.12 Temperature map at 61.2GHz for exposition times of 1s, 5s and 10s. 48
3.13 Relation between heating rate and power. 49
3.14 Time evolution of ΔT with input power of 0.1W, 0.5W, 1W and 5W. 50

List of abbreviations

- AP — Action Potential
- CNS — Central Nervous System
- CSF — Cerebrospinal Fluid
- EF — Endoneurial Fluid
- EHF — Extremely High Frequency
- EM — Electromagnetic
- FEM — Finite Elements Method
- HEK — Human Embryonic Kidney
- MMW — Millimetre Waves
- NFHL — Nerve Flexor Hallicus Longus
- PDMS — Polydimethylsiloxane
- PEC — Perfectly Electric Conductor
- PML — Perfectly Matched Layer
- PNS — Peripheral Nervous System
- RF — Radio Frequency
- RLN — Recurrent Laryngeal Nerve
- SAR — Specific Absorption Ratio
- Cl^- — Chloride Ion
- K^+ — Potassium Ion
- Na^+ — Sodium Ion

List of symbols

ρ_Q	Free charge density
ε_0	Dielectric constant of vacuum
μ_0	Magnetic permeability of vacuum
ε_R	Relative dielectric constant
$\tilde{\varepsilon}$	Complex permittivity
ε_S	Static permittivity (in Debye equation)
ε_∞	Permittivity at high frequency (in Debye equation)

μ_R	Relative magnetic permeability
σ	Electrical conductivity
σ^*	Complex conductivity
σ_S	Static ionic conductivity
c	Speed of light
γ	Propagation constant
α	Attenuation constant
β	Phase constant
δ	Skin depth
λ	Wavelength
v	Wave speed
k	Wave vector
ϕ	Relaxation function
τ	Relaxation time
ρ	Density
ρ_B	Blood density
E	Electric field
H	Magnetic field
D	Electric displacement
B	Magnetic flux density
P	Polarization
M	Magnetization
J	Free current

Abstract

Millimetre Waves (MMW) are a section of the electromagnetic (EM) spectrum in which there is a growing interest in various fields, like high speed wireless networks. Numerous studies were conducted on the possible effects of MMW on health since the 1960s and there is a considerable literature about the therapeutic effects of the *MMW therapy*, practised especially in the former USSR. The exact working principle is still not totally clear, but the main effect is believed to be of thermal nature.
Neural stimulation is widely used in therapy for the treatment of various disorders. The most diffuse technique is electric stimulation, but it presents limitations due to the current spreading which decreases selectivity. Another interesting approach is optogenetics which however requires gene therapy and it is still not proven on human models. For these reasons a novel neural stimulation device was studied which uses focused MMW as an alternative to electric stimulation, which does not require the expensive lasers used in optical stimulation or gene therapy and it could be easily miniaturized on an integrated flexible circuit.
The work is a feasibility study and consists mainly in a finite elements simulation of the thermal effects caused by the distribution of the electromagnetic field inside a model of the concept device. Selective stimulation was obtained by means of beamforming on the EM sources.
First a 2D model of a human sural nerve containing 12 fascicles was designed and the properties of the materials defined. For each tissue, the electrical properties were described by a 4-dispersion Cole-Cole model. Then 12 ideal EM sources were implemented in a circular array around the nerve, parametrized to be individually adjustable. For each simulation the electric field was solved and used as a heat source in the following bio-heat transfer study. All simulations were done at three frequencies: 35GHz, 61.2GHz and 122.5GHz.
The effect of the difference in electrical properties between the fascicles and the external connective tissue was investigated, compared with an homogeneous nerve tissue model. The ability to focus EM power in deep fascicles was found to be lower compared to focusing in superficial fascicles, so only this application was taken in consideration. The optimal number of active sources and thickness of a dielectric spacer to obtain the maximum power transfer was determined for

each frequency. The evolution of the temperature in a fascicle was simulated for an initial transient (100ms) and for longer stimulations (10s). The relation between the heating rate during the initial transient and the input power was calculated at four power levels (100mW, 500mW, 1W, 5W) and was found to be linear, which is consistent with the theory.
The initial studies suggest that the proposed device could find application in neural stimulation with the appropriate choice of parameters and input power, even though its performances would be lower than electric and optical stimulation as the thermal phenomena involved are slower. It might also be employed at low power levels for neural inhibition in pain therapy.

Chapter 1

Introduction

Electromagnetic (EM) waves are a constant presence in our everyday life, whether we are heating food in a microwave oven, downloading a video on our smartphones, having a phone call or even taking a stroll under the sunlight. We are constantly surrounded by invisible waves that, depending on their energy, interact in different ways with matter and give origin to electrical phenomena. The existence of electromagnetic waves was theorized by Maxwell in 1864 in his *Dynamical Theory of the Electromagnetic Field* in which are introduced for the first time the equations that describe the behaviour of electricity and magnetism, but his theory was limited to demonstrate the electromagnetic nature of light. It was Heinrich Hertz in 1888 that confirmed experimentally Maxwell's work, managing to generate and measure electromagnetic waves in laboratory. Hertz and his successors (commonly named the Maxwellians) expanded and rewrote Maxwell equations in the form they are known today [1]. EM waves are widely used in modern technology to transmit data and/or power from a device to another and they find applications in a multitude of fields such as RADAR detection [2], telecommunication [3] and heating [4]. Very interesting are the practical uses that EM waves find in the medical field, from imaging purposes [5, 6] to therapy by means of heating and power transfer [7, 8].
Millimetre waves (MMW) are electromagnetic waves in the frequency range of 30-300 GHz (often designated as Extremely High Frequency or EHF) having wavelengths of 10-1 mm. Numerous studies were conducted concerning the effects of low power MMW on biological tissues and possible health risks since the late 1960s. There is also a vast documentation on the use of MMW therapy in clinical practice (especially in the former Soviet Union) to treat a variety of diseases. [9–12] The exact theory behind the interaction of MMW with tissues has not been not fully understood: the principal mechanism is believed to be of thermal nature, but some theorize the presence of resonance-like effects which would explain the changes in neural excitability even at very low power levels. For this reason and for the lack of reproducibility of some of the experimental models,

the use of MMW in therapy was limited to the late USSR and other countries in Eastern Europe, being almost unknown in western science until recent years. The growing use of this band of the EM spectrum for wireless high-speed communication brought again concern for its possible biological effects, which renewed the interest in this field of the biomedical research.
Nerve stimulation is used widely in current medicine for the treatment and control of various pathologies and neurological disorders. The most diffused approach is *electric stimulation*, which provokes the excitation or inhibition of a nerve by injecting an external current. This method presents however limits regarding the selectivity of the stimulation, as the spreading of the current is difficult to control and nearby fibres could also be excited. In order to improve the therapeutic effect, various techniques are used to steer the current and obtain a more controlled effect.
Another promising approach is *optogenetics*, which is a technique where light is used to control the behaviour of excitable cells [13]. This is done by isolating a light sensitive protein (*opsine*) which can be either natural or chemically modified. It can be used as a ion channel and it responds to a particular wavelength. The expression of the light sensitive protein is achieved by means of gene therapy, usually with viral vectors. The cellular activity can then be controlled (excited or inhibited) with a particular pulsed light wavelength. This is achieved with implanted micro LEDs or by delivery with optic fibres.
The optogenetics approach for neural stimulation has a huge potential: it allows selective targeting of a determined neuron population with high spatial and temporal precision, it is not invasive and does not produce electrical artefacts on recording probes. It also allows to both excite and inhibit the same cells by using two different wavelengths, in a way that is more efficient that electrical inhibition. On the other side, it is difficult to express the the gene selectively on a specific cell section (like the axon membrane) and the selectivity is limited at targeting genetically different populations. There are also concerns that the stimulation modality is not completely physiological and risks to alter the functioning of the neural circuit. There are also issues in gene therapy that are not covered enough in literature so further testing should be done before it is possible to apply it to a human model [14, 15].
Selective stimulation refers to the activation of a specific nerve population without activating (and possibly inhibiting) the adjacent nervous fibres. It can be either the activation of fibres with the same diameter dimension (*fiber diameter selectivity*) or the activation of nerve fibres in a restricted region of space (*spatial selectivity*). This factor becomes more important when the nerve to be stimulated innervates different organs and a lack of selectivity may result in serious side effects.

1.1 Electromagnetic waves

In physics, a wave is a perturbation that carries energy without displacement of matter. It can be a mechanical or electromagnetic phenomenon or, in modern physics, can be associated with the motion of fundamental particles (electrons, photons, etc.). Mathematically speaking a wave is a function of both space and time. If the electric (or magnetic) sources vary in time, like an AC current inside a conductor, the fields also may depend on time. The equations for the stationary state, like Coulomb's law are not valid and the fields follow instead the four Maxwell equations [16]:

$$\nabla \cdot \mathbf{E} = \frac{\rho_Q}{\varepsilon_0} \qquad \text{Gauss' Law (electric)} \qquad (1.1)$$

$$\nabla \cdot \mathbf{B} = 0 \qquad \text{Gauss' Law (magnetic)} \qquad (1.2)$$

$$\nabla \times \mathbf{E} = -\frac{\partial \mathbf{B}}{\partial t} \qquad \text{Faraday's Law} \qquad (1.3)$$

$$\nabla \times \mathbf{B} = \mu_0 \left(\mathbf{J}_S + \varepsilon_0 \frac{\partial \mathbf{E}}{\partial t} \right) \qquad \text{Ampere's Law} \qquad (1.4)$$

E and **B** are the electric field and magnetic flux density in vector form, ρ_Q is the free charge density distribution and $\mathbf{J_S}$ is the free current density. These are the equations expressed in differential form and are valid both in vacuum and matter. Gauss' equations on the electric flux (1.1) and conservation of magnetic flux (1.2) remain valid in time dependent phenomena. Maxwell-Faraday's equation (1.3) tells that the presence of a variation in time of the magnetic flux induces a non conservative electric field. The potential induced in a closed loop is proportional to the rate of variation of the magnetic flux through the surface that the loop includes. Ampere's law (1.4) tells that the magnetic field induced around a loop is caused by two terms: the electric currents enclosed by the loop ($\mathbf{J_S}$, which is a source term) and the variation of the electric flux ($\mu_0 \varepsilon_0 \frac{\partial E}{\partial t}$, called by Maxwell *displacement current*).
The changing of the electric field generates a magnetic field and vice versa, so the two fields are strictly correlated. In fact from these equations Maxwell predicted the existence of electromagnetic waves travelling at the speed of light, the existence of which was confirmed later by Hertz [1]. Maxwell's equations are linear if the dielectric and magnetic medium are linear and the solutions follow the superposition principle: in presence of multiple sources, the total electric and magnetic field is given by the sum of the fields generated by each single source.
Inside a medium we should also account for the additional field components which are dependent on the material. These are the *polarization* (**P**) for the electric

field and the *magnetization* (**M**) for the magnetic field:

$$\mathbf{D} = \varepsilon_0 \mathbf{E} + \mathbf{P} \tag{1.5}$$
$$\mathbf{B} = \mu_0 \mathbf{H} + \mathbf{M} \tag{1.6}$$

The new fields are the electric displacement (**D**) which accounts for the effect of bound charges inside dielectrics and the magnetic field (**H**) which describes the magnetic driving force independently from the material magnetic properties. These fields are related to the electric field and magnetic induction through the *material equations*, which also introduce the relation between the electric field and the conduction current (**J**) in a medium of conductivity σ:

$$\mathbf{J} = \sigma \mathbf{E} \tag{1.7}$$
$$\mathbf{D} = \varepsilon_0 \varepsilon_R \mathbf{E} \tag{1.8}$$
$$\mathbf{B} = \mu_0 \mu_R \mathbf{H} \tag{1.9}$$

The effect of the polarization and magnetization are accounted for in two properties of the material: the dielectric constant (ε_R) and the relative magnetic permeability (μ_R).

Wave function

To obtain the electromagnetic wave equation, we take the curl of both sides in equation 1.3:

$$\nabla \times \nabla \times \mathbf{E} = -\frac{\partial}{\partial t}(\nabla \times \mathbf{B}) \tag{1.10}$$

From the vector identity

$$\nabla \times \nabla \times A = \nabla(\nabla \cdot A) - \nabla^2 A$$

and assuming a charge-free space so that $\nabla \cdot E = 0$ (from equation 1.4) we obtain:

$$\nabla^2 \mathbf{E} = \frac{\partial}{\partial t}(\nabla \times \mathbf{B}) \tag{1.11}$$

Substituting $\nabla \times \mathbf{B}$ with equation 1.4 and considering that the space is free of charges so there are no current sources ($\mathbf{J}_S$ = 0), we obtain the equation (in vacuum):

$$\nabla^2 \mathbf{E} - \mu_0 \varepsilon_0 \frac{\partial^2 \mathbf{E}}{\partial t^2} = 0 \tag{1.12}$$

Similarly for the magnetic flux density:

$$\nabla^2 \mathbf{B} - \mu_0 \varepsilon_0 \frac{\partial^2 \mathbf{B}}{\partial t^2} = 0 \tag{1.13}$$

These are *wave equations*, which have a generic form of the kind:

$$\nabla^2 f(r,t) = \frac{1}{v^2}\frac{\partial^2 f(r,t)}{\partial t^2} \tag{1.14}$$

where f is the amplitude of the wave, which can be a function of both space and time and v is the phase speed, which is the speed of propagation of the points with equal phase and in vacuum is equal to $1/(\sqrt{\varepsilon_0\mu_0}) = c$ (speed of light). Inside a medium the equations are the same but the wave speed is diminished because of the material, which usually has $\mu_R, \varepsilon_R \geq 1$, so $v = 1/(\sqrt{\varepsilon_0\varepsilon_R\mu_0\mu_R}) \leq c$. The most general case is the propagation of EM waves inside a lossy dielectric, which is a dielectric with a partially conducting medium ($\sigma \neq 0$) inside which the EM wave loses power because of ohmic dissipation. Inside a lossy dielectric the contribution of the conduction current ($\mathbf{J} = \sigma\mathbf{E}$, is not a source term) should be taken in consideration.
If the field are sinusoidal, it is convenient to express them as phasors:

$$E = E_0 \cdot e^{j\omega t}$$

this way the time derivative becomes a simple product for $j\omega$. Substituting in Maxwell equations 1.3 and 1.4, doing the same procedure as in equation 1.10 and following, considering the conduction currents generated in a medium (equation 1.7) we obtain:

$$\nabla^2\mathbf{E} - \gamma^2\mathbf{E} = 0 \tag{1.15}$$

$$\nabla^2\mathbf{B} - \gamma^2\mathbf{B} = 0 \tag{1.16}$$

where $\gamma^2 = j\omega\mu(\sigma + j\omega\varepsilon)$ is called *propagation constant*. Equations 1.15 and 1.16 are the wave equations and are called *Helmholtz equations* (in vector form). Since the propagation constant is a complex number, it can be written as the sum of two quantities:

$$\gamma = \alpha + j\beta \tag{1.17}$$

The real part α is called *attenuation constant* because it is a measure of the amplitude attenuation of the wave per unit length in the medium and is measured in nepers per metre (Np/m) or decibels per metre (dB/m).
The imaginary part is called *phase constant* because it is a measure of the phase shift of the wave per unit length and is measured in radians per metre (rad/m). The phase constant, the angular frequency and the speed of the wave are linked by the relation:

$$v = \frac{\omega}{\beta}$$

The two constants can be obtained considering the system of equations 1.18:

$$\begin{aligned} -\Re\{\gamma^2\} &= \beta^2 - \alpha^2 = \omega^2\mu\varepsilon \\ |\gamma^2| &= \beta^2 + \alpha^2 = \omega\mu\sqrt{\sigma^2 + \omega^2\varepsilon^2} \end{aligned} \tag{1.18}$$

which gives as results:

$$\alpha = \omega \sqrt{\frac{\mu\varepsilon}{2}\left[\sqrt{1+\left(\frac{\sigma}{\omega\varepsilon}\right)^2}-1\right]} \qquad \beta = \omega \sqrt{\frac{\mu\varepsilon}{2}\left[\sqrt{1+\left(\frac{\sigma}{\omega\varepsilon}\right)^2}+1\right]} \tag{1.19}$$

Another quantity of interest is the reciprocal of the attenuation constant α, which is called *skin depth* ($\delta = 1/\alpha$). It is a measure of the depth were the wave amplitude is reduced by a factor e^{-1} and is measured in metres.

Planar Waves

The most simple solution of the wave equation 1.14 is the planar wave equation. It is an equation of the kind:

$$E(r,t) = E_0 e^{j(\omega t - k\cdot r)} \tag{1.20}$$

where k is the wave vector, which is a vector parallel to the direction of propagation of the wave. $E(r,t)$ is expressed for convenience as a complex number, but only the real part of E has a physical meaning. For simplicity (but without loss of generality), we consider a wave propagating in the $\vec{z}$ direction, which only has a component along x, so: $E(r) = E_x(z)\vec{\mathbf{x}}$ (the time factor $e^{j\omega t}$ is implied in phasor notation). We substitute $E_x(z)\vec{\mathbf{x}}$ in Helmholtz equation 1.15 and we obtain:

$$\nabla^2 E_x(z) - \gamma^2 E_x(z) = \frac{d^2 E_x(z)}{dz^2} - \gamma^2 E_x(z) = 0 \tag{1.21}$$

This is a linear differential equation, with solution:

$$E_x(z) = E_0 e^{-\gamma z} + E_0' e^{\gamma z} \tag{1.22}$$

Considering that the second term implies a field of infinite amplitude for $z \to \infty$, it follows that $E_0' = 0$. Including the time dependency $e^{j\omega t}$, and remembering that $\gamma = \alpha + j\beta$, the planar wave equation is:

$$E(z,t) = \Re\{E_x(z)\cdot e^{j\omega t}\vec{\mathbf{x}}\} = \Re\{E_0 e^{-\alpha z} e^{j(\omega t - \beta z)}\vec{\mathbf{x}}\} \tag{1.23}$$

or in sinusoidal form:

$$E(z,t) = E_0 e^{-\alpha z} cos(\omega t - \beta z)\vec{\mathbf{x}} \tag{1.24}$$

In a similar way, we can solve Helmholtz equation 1.16 and obtain the wave equation for the magnetic field:

$$H(z,t) = H_0 e^{-\alpha z} cos(\omega t - \beta z)\vec{\mathbf{y}} \tag{1.25}$$

Note that the magnetic field is perpendicular to both the electric field (oriented in x) and the wave vector (oriented in z), so H must have a component only on the y direction.

1.2 Frequency behaviour of dielectrics

Biological tissues are lossy materials, which means their conductance is not negligible and it causes dielectric energy losses. Considering the simplest case, an homogeneous isotropic material between two conductive plates with surface A and height d (as in figure 1.1a), we can represent it with the electric equivalent in figure 1.1b.

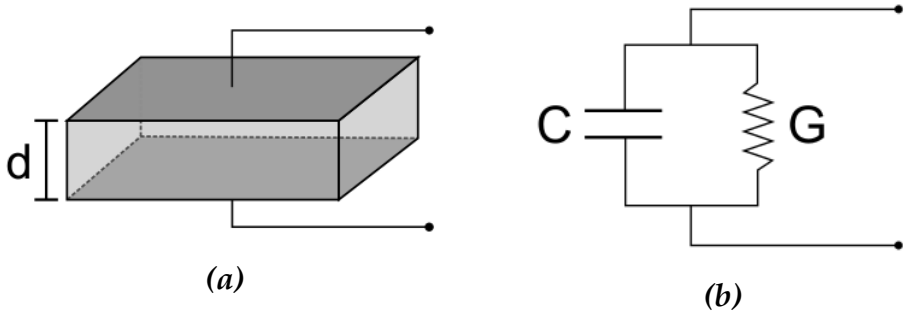

Figure 1.1: *Lossy dielectric (1.1a) and circuit equivalent (1.1b)*

Applying a sinusoidal field between the plates, we can define the complex admittance of the capacitance C in parallel to the conductance G

$$\begin{aligned} Y^* &= j\omega C + G = j\omega\varepsilon_0\varepsilon_R\frac{A}{d} + \sigma\frac{A}{d} \\ &= j\omega\frac{\varepsilon_0 A}{d}\left(\varepsilon_R - j\frac{\sigma}{\varepsilon_0\omega}\right) = j\omega C\cdot\tilde{\varepsilon} \end{aligned} \tag{1.26}$$

The term $\tilde{\varepsilon}$ is the *complex permittivity* of the dielectric. It can be written as a sum of a real term and an imaginary term

$$\tilde{\varepsilon} = \varepsilon' - j\varepsilon'' = \varepsilon_R - j\frac{\sigma}{\omega\varepsilon_0} \tag{1.27}$$

In the same way the *complex conductivity* can be expressed as

$$\sigma^* = \sigma' + j\sigma'' = \sigma + j\omega\varepsilon_0\varepsilon_R \tag{1.28}$$

The real part of the complex permittivity represents the dielectric constant $\varepsilon' = \varepsilon_R$ and is an indication of the energy stored inside the dielectric. The imaginary part of the complex permittivity instead represents the dielectric loss $\varepsilon'' = \frac{\sigma_s}{\omega\varepsilon_0}$ and is an indication of the energy dissipated in every cycle.

Relaxation

In non conductive medium, at molecular level, there are no free charges that can give origin to conduction currents. In polar substances (like water) are present instead electrical dipoles caused by a charge unbalance in the molecule. This dipoles are casually oriented and, in absence of an electric field, the mean value of the field generated by the dipoles is zero. If an external electric field is introduced, the effect on the dipoles is a torque moment that orientates them in the direction of the field. The contribution of the dipoles which are now parallel is summed and at macroscopic level it gives origin to the phenomenon of *polarization*. This affects the total electric field inside the medium, so a term is added to Maxwell equations

$$\nabla \times \mathbf{B} = j\omega\mu_0(\varepsilon_0\mathbf{E} + \mathbf{P}) + \mathbf{J} \tag{1.29}$$

where **P** is the polarization term due to the bound charges and **J** is the conduction current. When an electric field is applied, the dipoles do not orient themselves instantaneously but they do so according to a *relaxation function* $\phi(t)$ within a certain *relaxaton time* τ as in figure 1.2

$$P(t) = P_\infty + (P_0 - P_\infty) \cdot \phi(t) \tag{1.30}$$

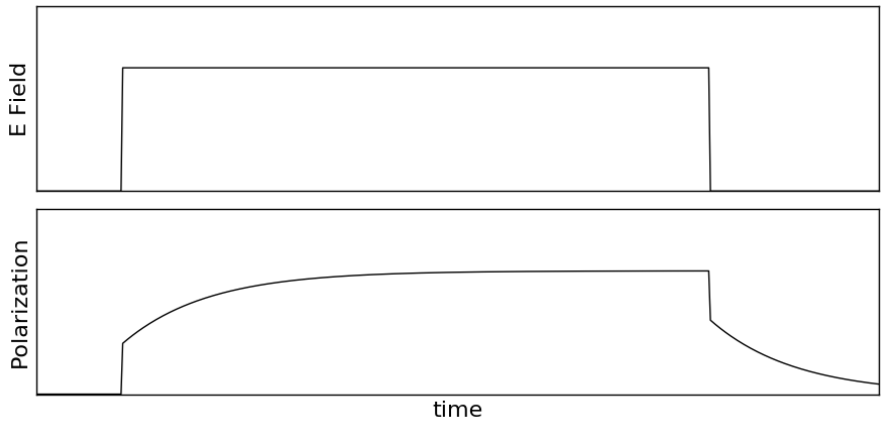

Figure 1.2: *The variation of polarization inside a dielectric is not instantaneous, but reaches a steady state after a relaxation time* τ

If we take the exponential function as relaxation function $\phi = (1 - e^{-\frac{t}{\tau}})$ and do a Laplace transform to express it in the frequency domain, we obtain the Debye dispersion formula

$$\tilde{\varepsilon} = \varepsilon_\infty + \frac{\varepsilon_s - \varepsilon_\infty}{1 + j\omega\tau} \tag{1.31}$$

Equation 1.31 represents the material complex permittivity ($\tilde{\varepsilon}$), ε_∞ is the permittivity at high frequency, ε_S is the static permittivity and τ is the relaxation time. By adding a term that considers the static ionic conductivity (σ_s), the Debye equation becomes

$$\tilde{\varepsilon} = \varepsilon_\infty + \frac{\varepsilon_s - \varepsilon_\infty}{1 + j\omega\tau} - j\frac{\sigma_s}{\omega\varepsilon_0} \tag{1.32}$$

We can then separate the real and imaginary part of the complex permittivity, ε' and ε'':

$$\varepsilon' = \varepsilon_\infty + \frac{\varepsilon_s - \varepsilon_\infty}{1 + (\omega\tau)^2} \qquad \varepsilon'' = \frac{\sigma_s}{\omega\varepsilon_0} + \frac{(\varepsilon_s - \varepsilon_\infty)\omega\tau}{1 + (\omega\tau)^2} \tag{1.33}$$

We can see that all these dielectric quantities ($\tilde{\varepsilon}(\omega)$, $\varepsilon'(\omega)$, $\varepsilon''(\omega)$) are dependent on the angular frequency ω.

The Debye first order model is not very representative of biological tissues since multiple dispersion phenomena are present at characteristic frequencies, each one with its relaxation time τ_i. The response of biological tissues can be modelled as a superposition of a number N of first order models:

$$\tilde{\varepsilon} = \varepsilon_\infty + \sum_{i=1}^{N} \frac{\Delta\varepsilon_i}{1 + j\omega\tau_i} - j\frac{\sigma_s}{\omega\varepsilon_0} \tag{1.34}$$

The Debye model does not always give an accurate representation of the behaviour of dielectrics, so certain variations were introduced for example in the Cole-Cole equation, which presents the term α ($0 < \alpha < 1$) that modulates the band width of the dispersion region:

$$\tilde{\varepsilon} = \varepsilon_\infty + \frac{\varepsilon_s - \varepsilon_\infty}{1 + (j\omega\tau)^{1-\alpha}} - j\frac{\sigma_s}{\omega\varepsilon_0} \tag{1.35}$$

Or in the Cole-Davidson equation, that introduces the term β ($0 < \beta < 1$), that produces an asymmetry in the dispersion band, shifting it towards higher frequencies:

$$\tilde{\varepsilon} = \varepsilon_\infty + \frac{\varepsilon_s - \varepsilon_\infty}{(1 + j\omega\tau)^{\beta}} - j\frac{\sigma_s}{\omega\varepsilon_0} \tag{1.36}$$

1.3 Millimetre waves in Therapy

In this section a brief collection of studies about the effects of MMW on biological tissues is presented.

Irradiation of low power MMW at 61.2 GHz on the skin of mice paw for 15 minutes showed a reduction of the pain perception, measured with the cold water tail-flick test. Transection of the sciatic nerve to desensitize the exposed area

eliminated the hypoalgesic effect, suggesting an interaction of MMW with the free nerve endings [17]. Radzievsky et al. found a relation between the MMW frequency and the hypoalgesic effect. It also showed the release of opioids in the hypothalamic area which is believed to be the principal cause of pain reduction [18].

Another study conducted on mice observed two effects: a decrease of the spontaneous electrical activity of the sural nerve during exposition to 45.2 GHz MMW (for incident power density ≥ 45 mW/cm^2) and a transient increase of the firing rate after the cessation of exposure that lasted 20-40s. The repetition of the experiment with a source of radiant heat reproduced the inhibitory effect but not the other one. It is hypothesized that the phenomenon involves cold receptors, since they have a similar behaviour at the end of an excitation [19].

A study done by irradiating mice brain cortical slices with 61 GHz MMW showed the same inhibitory effect followed by the transient increase but at power densities orders of magnitude smaller (284 - 737 nW/cm^2). During the exposition a reduction of the membrane input resistance of the neurons R_n up to 40% was also observed, calculated measuring the variation of membrane potential ΔV during the stimulation with the depolarization current ΔI [20].

In order to investigate the effects of MMW on more basic structures like the ion channels in the cell membrane, oocytes of the African clawed frog (*Xenopus laevis*) were exposed to 60 GHz MMW at power levels able to induce heating (4-128 mW) and changes in the ionic currents were measured. An increase in the kinetics of sodium and potassium channels was observed, consistent with heating effects [21]. Other studies on the effect of temperature on myelinated frog sciatic nerve showed a different phenomenon called *heat block*. It is demonstrated both theoretically with a simulation and empirically that a localized increase of temperature can suppress the propagation of an action potential [22].

1.4 Bio-heat transfer

The heat flow inside living tissues is complicated by several factors if compared with heat flow in non-living materials. First of all the blood perfusion adds a heat flow which is dependent on the shape and the dimension of the vessels network and on the blood temperature (which can be different from the tissue local temperature). The blood circulation itself is not always constant but depends on a variety of physiological and external factors. Another aspect to be considered is the heat generated by the metabolic processes inside the body [23]. Since heat is largely used for a number of medical applications [24], knowing the temperature distribution inside a tissue is a fundamental aspect. Temperature measurements with probes are invasive and only return a limited number of values in discrete points. For this reason a mathematical model is necessary to provide a more

accurate description of the temperature, which can be used to optimize the application.
The classic model employed for bio-heating problems was developed by Pennes in 1948 [25], which includes both the blood perfusion and the metabolic heating:

$$\rho C_P \frac{\partial T}{\partial t} = \nabla \cdot k\nabla T + \rho_B C_B \omega_B (T - T_0) + q_S + q_M \tag{1.37}$$

which describes the thermal variation over time ($\rho C_P \frac{\partial T}{\partial t}$) as the sum of the heat flow due to thermal conduction ($\nabla \cdot k\nabla T$), the heat flow due to blood perfusion ($\rho_B C_B \omega_B (T - T_0)$), the heat generated by sources (q_S) and the heat generated by metabolic reactions (q_M).
In the first term, ρ is the tissue density and C_P is the heat capacity at constant pressure. In the conduction term, k is the thermal conductivity and ∇T is the temperature gradient. In the blood perfusion, ρ_B is the blood density, C_B is the blood heat capacity, ω_B is the volumetric perfusion rate (defined as a volume unit of blood flowing in a volume unit of tissue per unit time, measured in s^{-1}) and T_0 is the blood temperature. Regarding the sources, if we consider electromagnetic heating we can calculate a time average of EM power: $q_S = q_{EM} = \frac{1}{2}\sigma|E|^2$.
Both the metabolic term (q_M) and blood perfusion are considered to be distributed homogeneously in the tissue and isotropic.

1.5 Nervous System

The nervous system is tasked with a fundamental activity for the human body: the communication with the external world. It receives a multitude of information from the surroundings and from the body, it elaborates them and provides the adequate response by means of actuators, which can be either muscles (movement) or glands (secretion).
The nervous system is organized in a Central Nervous System (CNS) composed by the brain and spinal cord, and Peripheral nervous System (PNS) composed by the neurons and ganglia outside the brain and spinal cord. The nervous system is mainly composed by two kinds of cells: neuroglia and neurons. Neuroglia or glial cells are all the cells that provide to the homeostasis and support of neurons, form the blood-brain barrier and produce the myelin. Neurons are a kind of cells highly specialized for information processing in the form of electrical signals. This is done by receiving the information, transporting it for a certain distance and then transmitting it to other neurons. A neuron cell is composed of a central body (soma) that contains the nucleus and is the metabolic center and the source of most of the substances contained inside the cell. From the soma departs a

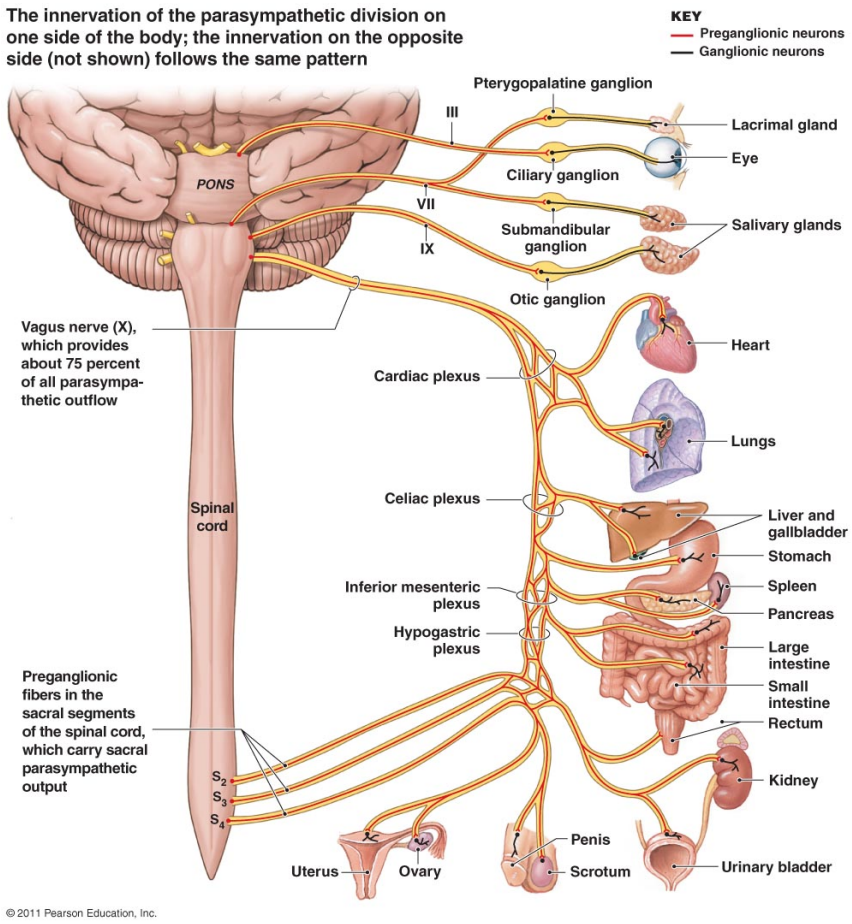

Figure 1.3: *Nerves of the parasympathetic system on the right side of the spine. Notable is the vagus nerve (X), which innervates most of the major organs. In nerves like this one, selectivity is very important for nerve stimulation. Figure taken from [26]*

long and thin ramification (the axon) which conducts the information going outside the cell and several shorter branches (the dendrites) which receive the information from external sources. These ramifications terminate in small swellings called synaptic boutons. Nervous cells are linked to one another by means of *synapses* which transmit the information either electrically or (more commonly) chemically. The number of synapses far exceeds the total number of neurons in a human body.

A nerve is composed by a great number of axons, which are surrounded by a layer of connective tissue called *endoneurium*, containing also the capillaries for the nourishment of the nerve. Axons are then grouped in fascicles, surrounded by a hard fibrous membrane called *perineurium*. The whole nerve is composed by different fascicles surrounded by a connective membrane called *epineurium* which

can be divided in an internal epineurium, surrounding the single fascicles and an external epineurium, surrounding the whole nerve and containing blood vessels (see figure 1.4). [27, 28]

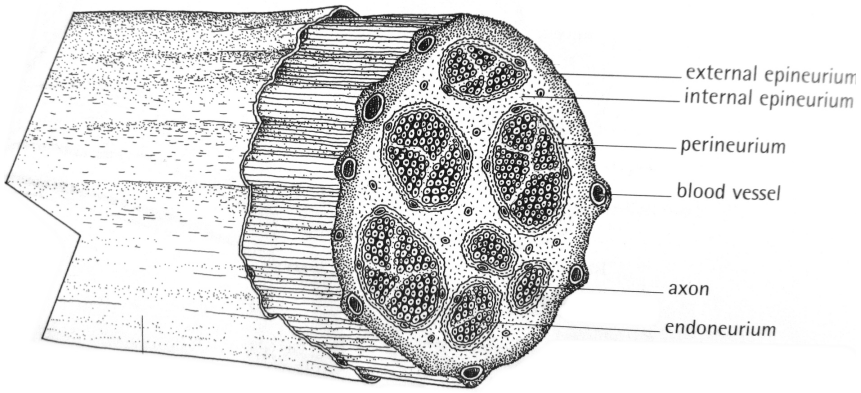

Figure 1.4: *Anatomy of a nerve. The axons are grouped in fascicles and contained in the epineurium. The fascicles are delimited by the perineurium and are surrounded by the internal epineurium. The external perineurium surrounds the entire nerve. Image taken from [29].*

Neurons can be covered by an insulating myelin sheet which is a fatty membrane that blocks the diffusion of ions through itself, increasing the conduction speed of the nerve up to 20 times. The myelin sheet is produced by glial cells called Scwann Cells and is interrupted in spots called *nodes of Ranvier*. Nerve fibres can be divided in three types, based on the axons diameters (d) and the presence or absence of the myelin sheet [30]:

- **A fibres**, which are large myelinated fibres and have high conduction speed. They are further divided in Aα (d = 12-22μm, v = 70-120m/s), Aβ d = (5-12μm, v = 30-70m/s), Aγ (d = 2-8μm, v = 15-30m/s) and Aδ (d = 1-5μm, v = 5-30m/s).
- **B fibres**, which are less myelinated than A fibres with diameters of less than 3μm and conduction speed of 3-15m/s
- **C fibres**, small unmyelinated fibres with diameters of 0.1-1.3μm and conduction speed of 0.6-2m/s

Action Potential

The nervous pulse conduction inside a neuron is different from the current flowing inside an electric conductor, which is caused by an ordered movement of

charge carriers. In a neuron the pulse, called *Action Potential* (AP) is caused by the flow of ions through the cell membrane (figure 1.5). When a neuron is not excited, the concentration of Na^+, Cl^- and K^+ ions between the inside and the outside of the membrane is very different, which gives origin to a *resting potential*. The cell membrane is a barrier to the movement of ions, which can only pass through special membrane channels which are sensitive to various stimuli (electrical, chemical and mechanical). When the resting potential grows over a certain threshold the membrane is depolarized and Na^+ channels open, letting the ions flow following the concentration gradient and causing an inversion in the membrane polarity. Then, after the potential has reached the maximum value, the Na^+ channels close and the K^+ channels open causing an ion flow in the opposite direction, re-polarizing the membrane and restoring the negative potential. After an AP, the membrane is slightly hyperpolarized for a short time called *refractory period* during which no action potential can be generated. The Action potential propagation happens like a cascade reaction from the excitation point: the AP itself depolarizes the following section of the cell membrane causing the opening of the voltage-gated ion channels, while the backward propagation is prevented by the hyperpolarization of the previous membrane section during the refractory period. Neurons covered by the myelin sheet have a higher conduction speed since the depolarization is not continuous but "jumps" from node to node [28].

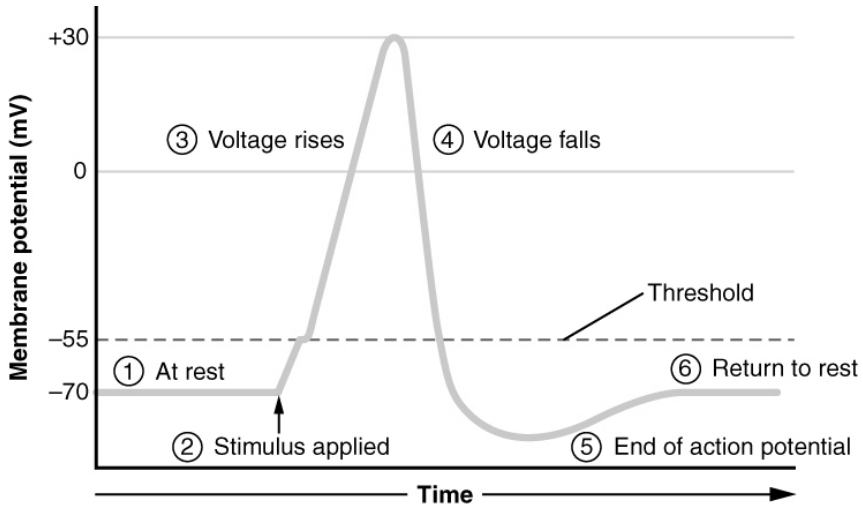

Figure 1.5: *Plot of the membrane voltage during an action potential. 1) Resting potential. 2) A stimulus is applied, the Na^+ gates open and the membrane depolarizes. 3) The potential goes over the threshold, the Na^+ enters the membrane very quickly. 4) The K^+ gates open and ions flow outside the membrane, lowering the potential. 5) The K^+ channels remain open and the membrane is hyperpolarized. 6) Return to resting potential. Figure taken from [31].*

1.6 Neural Stimulation

Electrical nerve stimulation is a widely used therapy for the treatment of different neurological disorders, like vagus nerve stimulation for the treatment of epilepsy [32,33] and electrical nerve stimulation for the treatment of pain [34,35]. It can also be employed in functional restoration and neural prosthetic to restore sensory and motor systems in impaired individuals. Some examples are visual prostheses and cochlear implants [36, 37], bladder control for paraplegics [38] and motoneuron stimulation for restoring movement in subjects paralysed after a stroke or spinal cord injury [39].
A critical aspect regarding neural stimulation is the selectivity: inside a nerve trunk are contained numerous fibres with different diameters, both afferent and efferent, which carry out different functions. This causes non-trivial issues as the stimulation threshold for the smaller fibres can be 2 to 100 times higher than larger fibres, of which the activation is not always desired. For example the vagus nerve contains both parasympathetic efferent fibres and visceral afferent sensory fibres originating from the head, neck, thorax and abdomen [40]. In this case fibre diameter selectivity is more relevant as the cardioinhibitory fibres in the vagus nerve are the small B and C fibres, while the stimulation of the A fibres branching to the laryngeal nerve can cause undesired side effects like hoarseness [41].
Considering the state of the art in electrical stimulation, there are different approaches to control the stimulation selectivity. Regarding the fibre diameter selectivity the approach consists in using particular stimulation waveforms:

- **Burst-modulated waveform**, which also increase the charge injection efficiency. The stimulation parameters can be adjusted to increase the C fibres selectivity or the A fibres selectivity [43].

- **Rectangular current pulses** produce a lower stimulation threshold for large fibres compared to small fibres, so they can be used to stimulate large fibres selectively [44].

- **Long hyperpolarizing pulse** (anodic) can block the fibres conduction. Large fibres are blocked more easily than small fibres. In peripheral nerves it gives origin to the phenomenon of *anodic break* (generation of an action potential at the end of an hyperpolarization), so a slowly decaying pulse is preferred. It can be used to achieve one-directional conduction or small fibres stimulation (by blocking the large fibres) [44].

- **Quasi-trapezoidal** current pulses were used to differentially block motoneurons obtaining a physiological muscle fibres recruitment to modulate muscle force [45].

Regarding spatial selectivity, the main approach consists in an appropriate electrode design:

- An **electrode array** is used, since the electric field is stronger near the active electrode (it is roughly proportional to r^2) and the stimulation threshold are lower [44].
- The **tripole** configuration of the stimulation electrodes allows to contain the current better than with monopolar stimulation, exciting preferentially the fibres near the surface [46].
- The use of a transversal **sub-threshold steering current** was proved to improve the spatial selectivity both in monopolar and tripolar configuration [46, 47].
- Two **adjacent tripoles** in parallel, with a transversal steering current allowed to stimulate selectively nerve fascicles that could not be activated individually with a single tripole and steering current [47].
- The use of a **flat interface nerve electrode** (**FINE**) allows a certain degree of reshaping of the nerve without injuring the nerve fibres. The reshaping gives easier access to the neurons and improves spatial selectivity with monopolar stimulation (the results are comparable to tripolar stimulation with steering current) [48].

The non-linear behaviour of the membrane can also be employed to enhance the selectivity by changing the excitability of the fibres [44]:

- An **hyperpolarizing pre-pulse** raises the excitability of the neuron right after the application. The effect is stronger near the electrode and on large fibres, so it increases both the spatial selectivity and fibre diameter selectivity.
- A **sub-threshold depolarizing pre-pulse** lowers the excitability of the neurons right after the application. This effect is stronger near the electrode and on large fibres, so it can be used to stimulate more easily distant fibres and inactivate large fibres.

Electromagnetic stimulation with Millimetre waves (MMW) is potentially easier to control than electric currents, allowing better spatial resolution by means of beamforming and wave focusing. The small wavelength (of the order of few mm) is further reduced by the high dielectric constant of the tissues. It is also cheaper and more practical than optical stimulation and the device can be miniaturized on an integrated circuit and implanted. A concept of such a device is shown in figure 1.6. The principles of MMW stimulation are based on the assumption that

the effects on tissues (seen in section 1.3) are of thermal nature.
Wells et al. [49] stimulated the sciatic nerve of a frog *in vivo* with low intensity infra-red laser pulses obtaining leg muscle contraction. The experiment was subsequently validated on Sprague–Dawley rats, using electrical stimulation as a standard for comparison. They concluded that the mechanism of optical stimulation is not yet understood but hypothesize a thermal mechanism is responsible for the opening of the membrane ion channels.
In a later study [50] Shapiro et al. have observed that in oocytes exposed to infra-red laser pulses a depolarizing current is generated, which can be correlated with the temperature increase. The same effect was also observed in whole cell clamped HEK cells. They hypothesized that the membrane capacitance was dependent on the temperature, which was later confirmed by experiments on an artificial lipid bilayers exposed to infra-red laser pulses. The artificial membranes exposed to laser are subject to a capacitance increase, with decaying times of 100-200ms, which are consistent with thermal relaxation. By taking advantage of this property, we can obtain membrane depolarization by changing the membrane passive capacitance (which is independent from the membrane ion channels).

1.7 Objective

The objective of this thesis is to conduct a feasibility study to investigate if it is possible to achieve selective neural stimulation with a physical principle different from electrical stimulation. We hypothesize that it is possible to depolarize a nerve membrane with the application of heat, induced by focusing MMW on a spot. The principal points that were dealt with in this study are:

- The design of a model of the nerve representing the anatomy and tissues composition as accurately as possible and comparison with an homogeneous model.
- The ability to focus in deep or superficial fibres.
- The influence of various parameters (frequency, number of EM sources, thickness of dielectric spacer, input power, irradiation time).

1.8 Materials and methods

The main part of the work consists of a finite elements method (FEM) simulation of the nerve-antenna system realized using the COMSOL [51] software (v.5.1). Additional processing of data and calculations were made with the use of GNU-Octave [52] environment (v4.0) and Python [53] programming language (v.2.7.12),

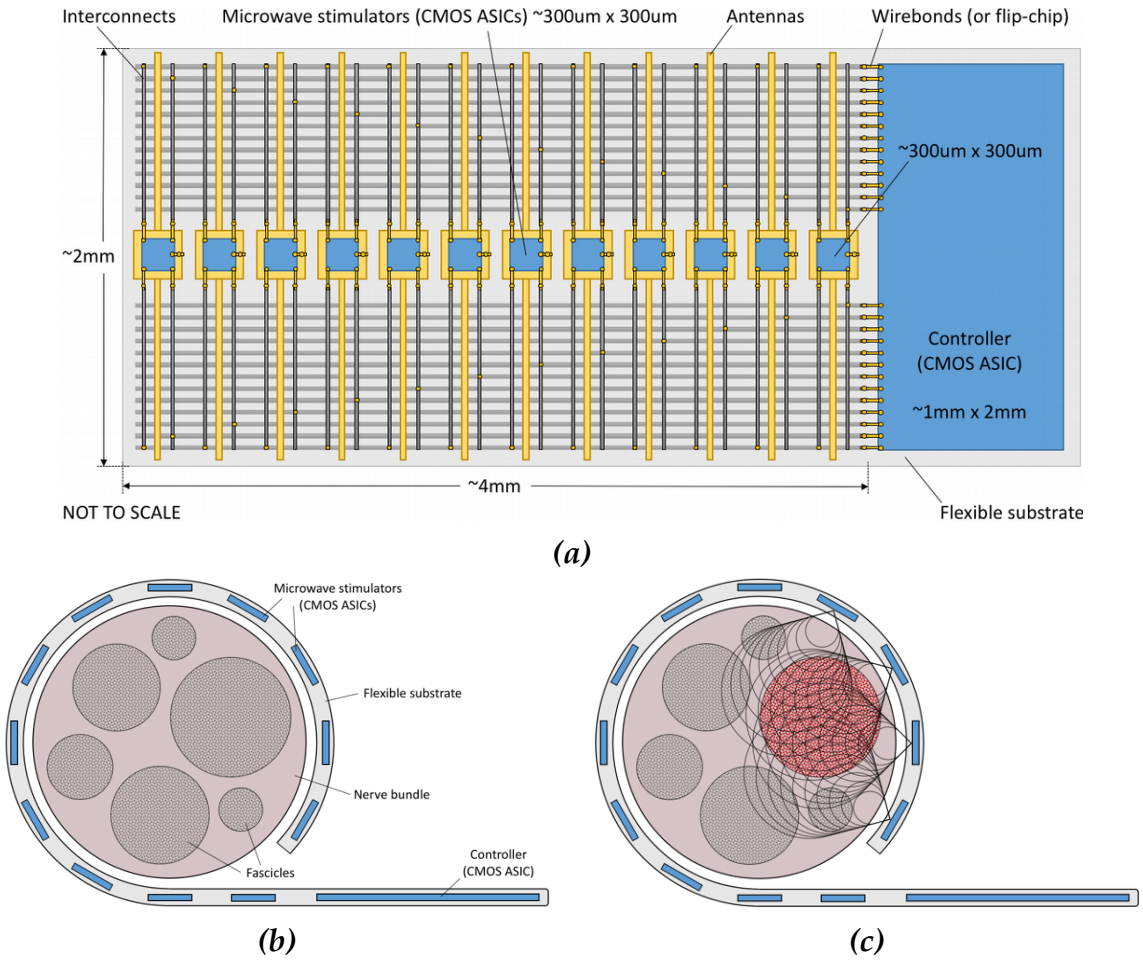

Figure 1.6: *Concept of the hypothetical device. (1.6a) Micro antennas and CMOS integrated controllers embedded on flexible substrate. (1.6b) cross section of the cuff wrapped around the nerve. (1.6c) selective stimulation using phased arrays. Figure reprinted with permission.*

which was also used to generate most of the graphs. Measurements on histological pictures were done with free ImageJ software [54] (v.1.51j8).

Chapter 2

Nerve Model

In order to start with the simulations a model of the nerve was initially developed, including the dielectric properties of the tissues and its morphology. For our purposes we considered a peripheral nerve of medium diameter (2mm) to explore the capabilities of wave focusing. Some simplifications were done, like considering the tissue isotropic (an acceptable assumption at high frequencies) and approximating the geometries with perfect circles. In order to run the FEM electromagnetic simulation the materials should be first electrically and magnetically characterized, specifying their conductivity (σ), dielectric constant (ε_R) and magnetic permeability (μ_R). In biological tissues these values are often complex and frequency dependent, so different models were developed in order to model their behaviour (see section 1.2).
The FEM simulations were made with the RF module and bio-heat module of COMSOL Multiphysics [51]. The RF module has a study in the frequency domain (stationary state). All the dimensions are expressed as phasors and the frequency is supposed to remain constant. It solves iteratively Maxwell's equations in vector form and gives as results the electric and magnetic fields. The bio-heat module has a time-dependent study, which means the solutions are computed for a discrete number of time steps. It is used to solve Pennes bio-heat transfer equation, using the EM fields computed by the RF module as a heat source and obtaining the temperature as solution.

2.1 Gabriel model

The simplest model is a homogeneous and isotropic tissue. The tissue electrical properties were taken by a parametric model developed by Gabriel [55], which is used as reference for bio-electric applications. It is a variation of the Cole-Cole model including 4 dispersion regions. Since there are not a lot of measurements

done on biological tissues at very high and very low frequencies, the values obtained with this model should be used with caution in the present study on frequencies ranging 30-300GHz, as the actual behaviour might be significantly different. The complex relative permittivity of the tissue is expressed as:

$$\varepsilon_R^*(\omega) = \varepsilon_\infty + \sum_{n=1}^{4} \frac{\Delta\varepsilon_n}{1 + (j\omega\tau_n)^{(1-\alpha_n)}} + \frac{\sigma_i}{j\omega\varepsilon_0}$$

In which ε_∞ is the permittivity at terahertz frequencies, σ_i is the static ionic conductivity while $\Delta\varepsilon_i$ and τ_i are respectively the drop in permittivity and the relaxation time for each of the four dispersion regions. The Cole-Cole equation introduces also the distribution parameter α_i to the Debye equation, which is a measure of the dispersion in each band.
If we consider that $\varepsilon_R^* = \varepsilon_R - j\frac{\sigma}{\varepsilon_0\omega}$ the dielectric properties ε_R and σ are then calculated using the parameters $\Delta\varepsilon$, τ and α derived by experimental data by Gabriel and Gabriel [56]:

$$\varepsilon_R = \Re\{\varepsilon_R^*\} \qquad \sigma = -\Im\{\varepsilon_R^*\} \cdot \omega\varepsilon_0$$

Regarding the magnetic permeability of the nerve, we can approximate almost every soft tissue in the body with the value of water ($\mu_R = 1$). Figure 2.1 shows the dependency of σ and ε_R with the frequency.

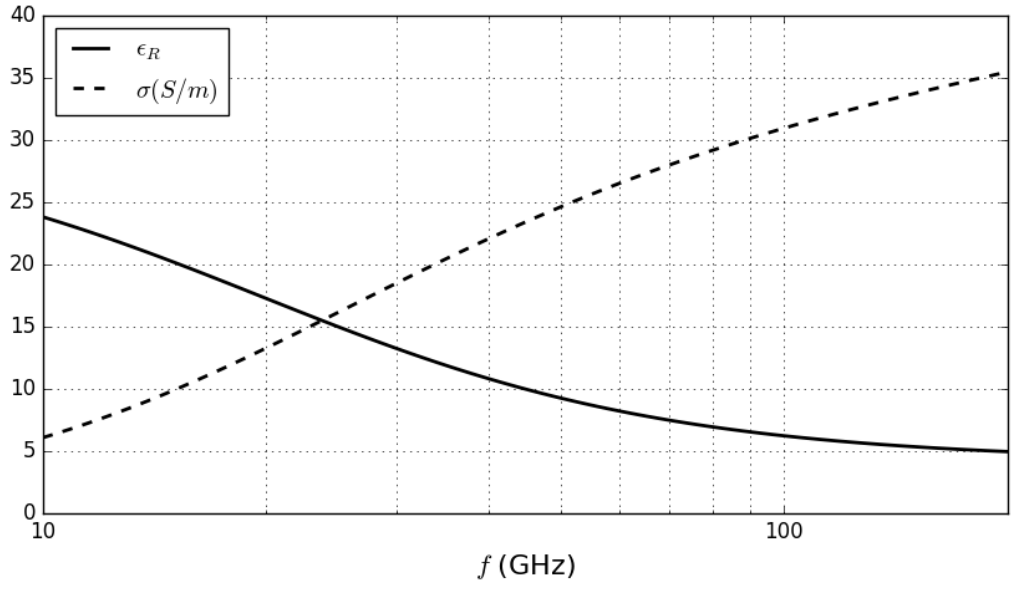

Figure 2.1: *Frequency dependence of dielectric properties of the nervous tissue in the range 10 - 200GHz*

2.2 Anatomical Model

The homogeneous model is simple but not accurate. The presence of different tissues with different electrical properties inside a nerve might generate phenomena of reflection and diffraction of incident waves, reducing this way the ability of focusing EM energy. A difference in electrical conductivity can also influence the rate of EM heating.

Tissues

In order to make a model closer to the nerve anatomy (discussed in section 1.5) two different tissues were considered for the model: the *epineurium* which is dense connective tissue surrounding the fascicles and the *endoneurium* which consists on the extracellular fluid surrounding the axons and the myelin sheets. Different studies have been conducted to determine the composition of the connective tissue in nerve fibres. A summary of the literature follows.

Epineurium: is primarily composed of collagen fibres and adipose tissue. There may be present also elastin fibres but since their quantity is modest we will neglect their contribute. In some nerves the epineurium can be divided in a inner part, surrounding each fibre, and an outer part, surrounding the bundle of fascicles. For our purpose we will only consider the presence of an inner epineurium.

- The percent of fat tissue in the epineurium of the Recurrent Laryngeal Nerve (RLN) was compared with the one in Nerve Flexor Hallicus Longus (NFHL) in dog [57]. The mean values were $(47 \pm 16)\%$ in RLN and $(31 \pm 15)\%$ in NFHL in male dogs. The values of adipose tissue in female dogs were 10% higher.

- The composition of sural nerve from eight cadaveric samples was investigated [58]. The percentage of fat inside the epineurium was calculated to be $18.2 \pm 14.4\%$. The lower value with respect to the findings in [57] might be caused by the post-mortem nature of the tissues and their preparation method.

Endoneurium: is the part of the nerve surrounded by the perineural membrane. It contains the axon bodies, loose connective tissue and extracellular fluid [59]. For our purpose we will neglect the presence of vessels and other kinds of cells such as fibroblasts, macrophages and Schwann cells.

- In [59] the composition of the endoneural space is reported as following: 24-36% of volume is occupied by myelinated fibres, 11-12% by unmyelinated fibres, 35-45% by collagen and the remaining 12-14% by water and macromolecules.

- Sural nerve trunks from 10 volunteers aged 9-80 years were examined [60]. The mean CSA of the whole nerves was found to be $2.3 \pm 0.8mm^2$, with no statistically difference between the two age groups (9-51 years and 52-80 years). The percentage of endoneurium volume occupied by myelinated axons changes between the two groups, from $(33.5 \pm 12.4)\%$ in the first to $(14.3 \pm 8.6)\%$ in the second.

Based on these studies, a reasonable choice of parameters for the materials was made:

Epineurium: 30% adipose tissue, 70% collagen;

Endoneurium: 45% nerve fibres, 40% collagen, 15% endoneurial fluid;

Dielectric Properties

Once the composition of the materials had been defined, the dielectric properties of the tissues were investigated. This was not a trivial process as most biological tissues have properties which are dependent on the frequency (as already seen in section 1.2) and the literature on biological tissues at microwaves is scarce. Some approximation were made with the data available:

- Collagen tissue was extrapolated from tendon tissue. This is reasonable since tendons (excluding water content) are composed of collagen up to 90%. The remaining 10% are elastin fibres, proteoglycans and various kinds of inorganic components. The collagen is prevalently Type I collagen (97-98%) with small amounts of Type III and Type V collagen.

- The values for fat tissue are taken from subcutaneous fat.

- The endoneurial fluid (EF) was modelled as cerebrospinal fluid (CSF) since they have the same physiological function. The EF however has concentrations of electrolytes more similar to blood plasma, so they should be slightly higher than in CSF.

- The dielectric properties of axons are measured on whole spinal nerve fibres, so they already include the connective tissues.

All the tissues are modelled with the Gabriel parametric model [55], saw in section 2.1. The tissue in question are respectively: *Tendon*, *Fat (non infiltrated)*, *Cerebrospinal Fluid* and *Nerve*. In figure 2.2 the dielectric properties of tissues between 10GHz and 200GHz are compared. In table 2.1 are reported the values of ε_R and σ of the three tissue models at some relevant frequencies.

	Nerve (Gabriel)		Epineurium		Endoneurium	
frequency (GHz)	ε_R	$\sigma(S/m)$	ε_R	$\sigma(S/m)$	ε_R	$\sigma(S/m)$
35	11.8	20.4	9.2	18.9	13.4	27.3
42.2	10.4	22.7	8.0	20.4	11.6	29.9
53.6	8.8	25.3	6.8	22.0	9.7	32.9
61.2	8.1	26.7	6.3	22.8	8.8	34.5
78	7.0	28.9	5.6	24.2	7.5	37.0
100	6.2	30.9	5.1	25.5	6.6	39.3
122.5	5.7	32.4	4.7	26.4	6.0	41.0
150	5.3	33.7	4.5	27.3	5.5	42.6

Table 2.1: *Dielectrical properties of Gabriel's nerve model and the two connective tissues model at some relevant MMW frequencies.*

Geometry

The model geometry was based on an histological picture of the cross-section of a sural nerve, taken from [60]. The picture is ideal for the purpose: the tissues are easily identifiable and nerve and fascicles have roughly a circular shape. The nerve has a diameter of 2mm and contains 12 fascicles that can be divided into three size categories: small (0.15 - 0.17mm, 4 fascicles), medium (0.25 - 0.33mm, 5 fascicles), big (0.43 - 0.48mm, 3 fascicles). The image was imported inside a vectorial CAD software and the outlines of nerve and fascicles traced, approximating them with circles (see figure2.4a). The path was then saved in various vectorial formats like .dxf and .svg for importing in COMSOL.

2.3 2D models and mesh

The nerve model dimensions are based on the sural nerve seen in figure 2.4. Two models were built in parallel: the homogeneous Gabriel Model seen in section 2.1 and the anatomical model in section 2.2 (figure 2.5). The two nerves have the same radius (1mm) but the homogeneous model does not have two different materials for the fascicles and connective tissue. Around the nerve are wrapped a dielectric spacer of variable thickness (controlled by a parameter) and a flexible insulating substrate of thickness $50\mu m$. The dielectric spacer is a low-loss insulating layer which has a dielectric constant matching the one of the tissue. Its purpose is to reduce the dissipation in the near reactive field, improving this way the power transfer [61, 62]. Having same dielectric constant, the reflections at the interface are also reduced. The external domain has a radius of 3mm, terminating in a Perfectly Matched Layer (PML) of $200\mu m$. The PML introduces a complex transformation that attenuates the incident waves and is used to avoid

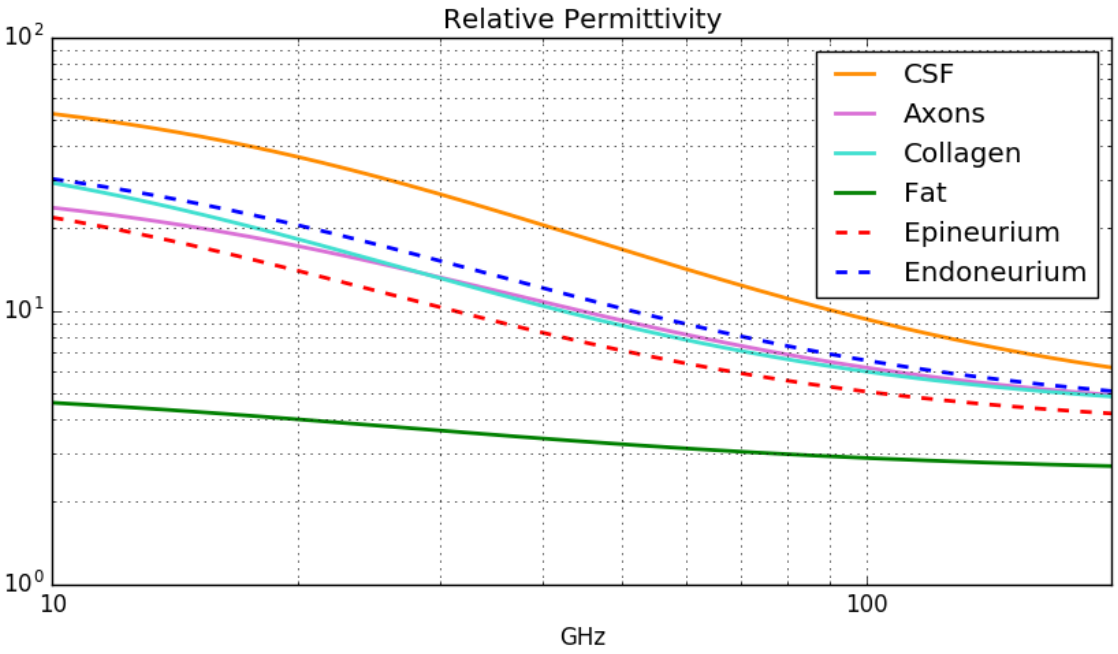

(a)

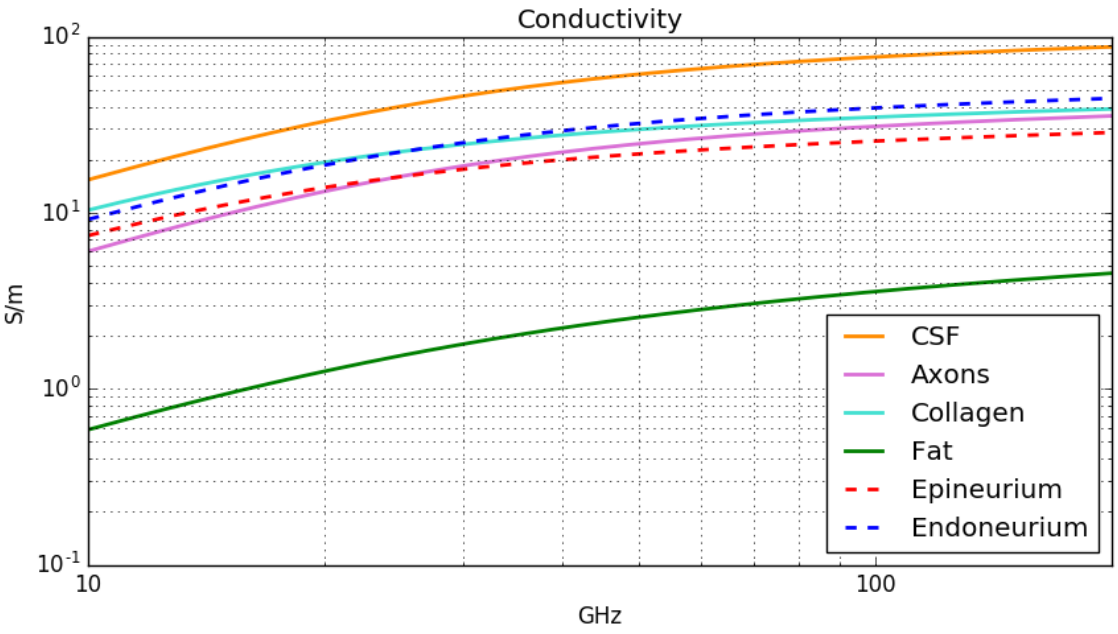

(b)

Figure 2.2: *Comparison of relative permittivity (2.2a) and conductivity (2.2b) of tissues and models of epineurium and endoneurium in the frequency range 10 - 200GHz.*

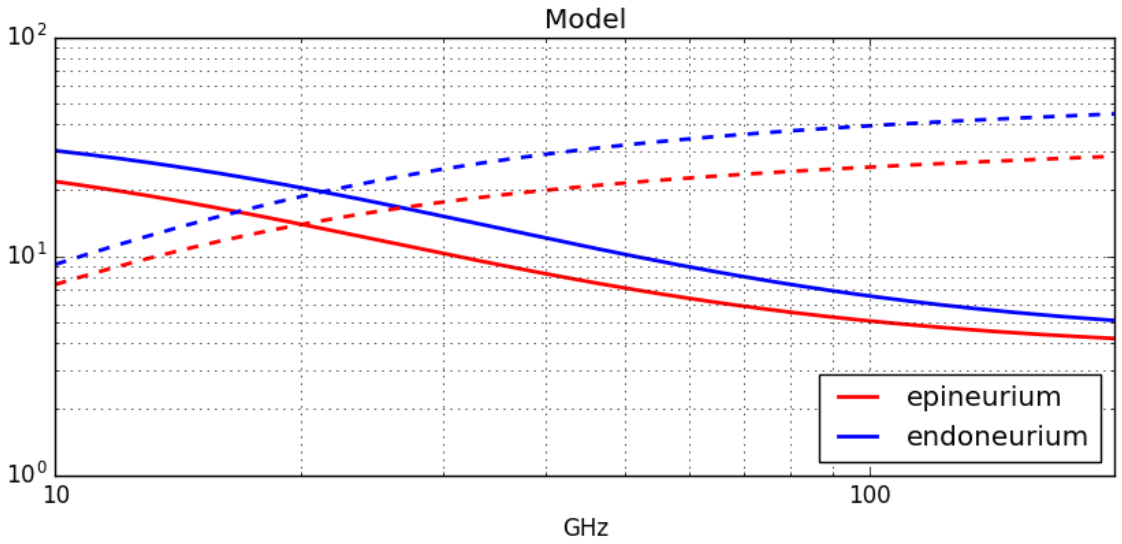

Figure 2.3: *The relative permittivity (solid line) and conductivity (dashed line, in S/m) of the two connective tissues are compared.*

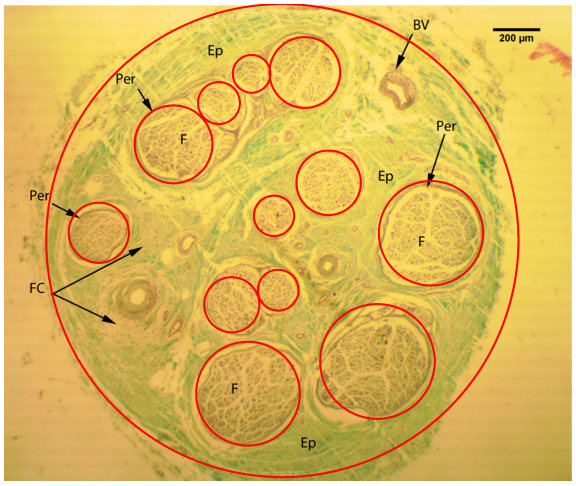

(a) *Cross section of human sural nerve. The image was imported in CAD software and traced with circles (in red). The scale is* $200\mu m$*. Image from [60].*

(b) *3D model obtained by extruding the nerve profile by 5mm.*

Figure 2.4

reflections back inside the model, approximating this way the behaviour of an open boundary medium [63]. The Electromagnetic sources were modelled as almost planar surfaces from where the EM waves enter the model, their width is

also parametrized. In this study 12 sources were used, numbered starting from the top one and moving clockwise.
The geometry was then meshed with free triangular elements, adjusting the dimensions manually where more accuracy was necessary (for small details). The PML also requires a particular type of elements, as it can be seen in figure 2.6.
It should also be noticed that in 2D COMSOL treats the z-dimension as if it was of unitary length (1m) which is very large compared to our model. We will consider a nerve section of about 1mm, so that all the quantities that require a z component (volumetric or boundary surfaces) will actually be 1000 times smaller than the simulation parameters (for example, an input power in a port of 1W will actually be 1mW). In the following, all these dimensions refer to the already scaled quantities.

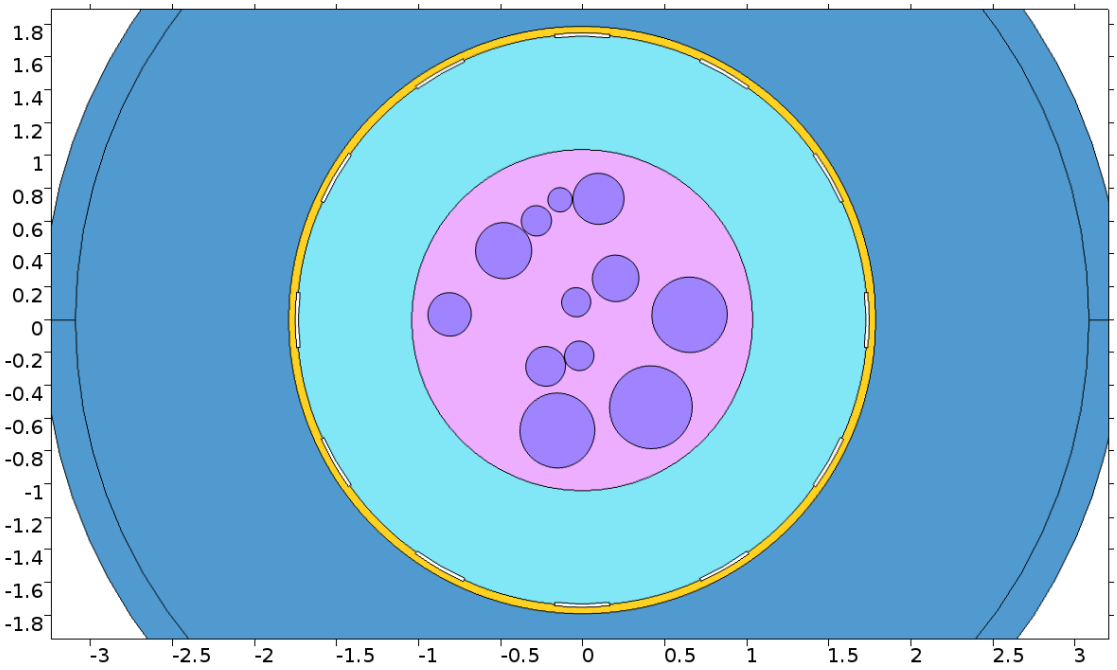

Figure 2.5: *The geometry of the model. Starting from the center we have the nerve with fascicles (r=1mm), the dielectric spacer (h = 500μm), the flexible substrate (h = 50μm), the external domain (r=3mm) and the PML(h = 200μm). The axes are in mm.*

2.4 Materials

The next step is to define the materials used in the model, which means that we need to characterize electrically every domain by defining the values of conductivity (σ), dielectric constant (ε_R) and magnetic permeability (μ_R).

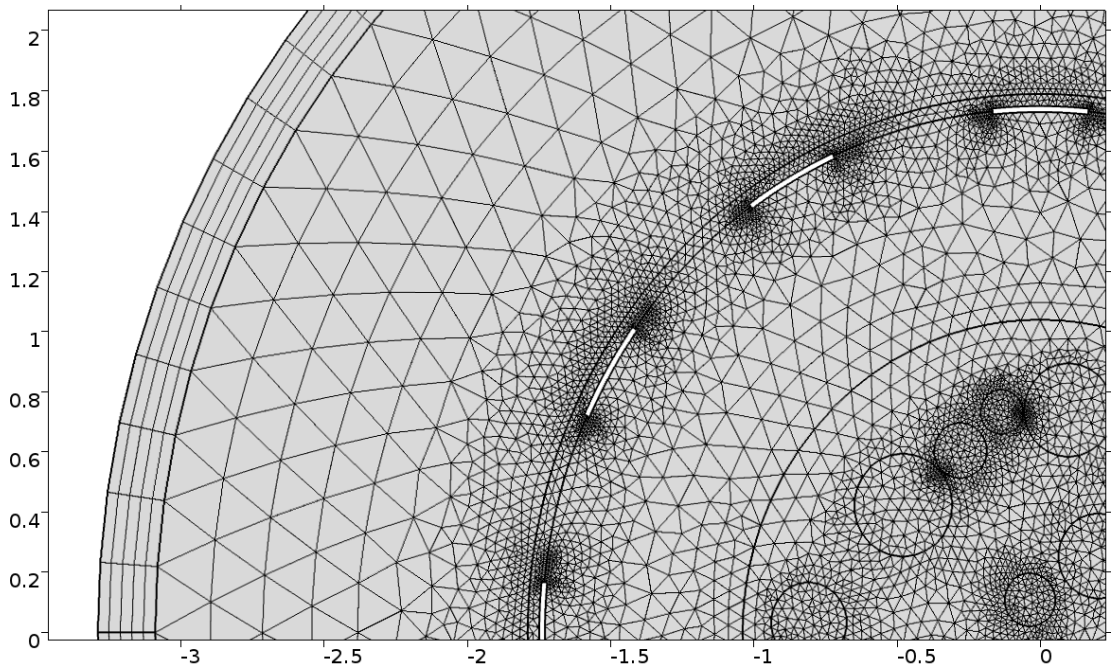

Figure 2.6: *Detail of the meshed model. All the model uses free triangular elements, except for the PML which requires square elements, perpendicular to the expected incident waves. The axes are in mm.*

- The nerve electrical properties are dependent on the frequency and are taken from Gabriel's [55] for the homogeneous model. The properties of epineurium and endoneurium derive from the model developed in section 2.2 for the anatomical model.
- The dielectric spacer has the same dielectric constant of the underlying tissue (nerve in the Gabriel model, epineurium in the anatomical model) but it is a material without losses ($\sigma = 0$). Its purpose is to reduce the ohmic losses in the near field and the reflection at the interface, optimizing the power transfer inside the tissue [61, 62].
- For the flexible substrate PDMS was chosen. Its dielectric properties are $\varepsilon_R = 2.75$ and $\sigma = 2.5 \cdot 10^{-14}$ S/m [64].
- The properties of the external domain were considered less important for the purposes of this work, so a simple Debye model of water was implemented (formula 1.31). Parameters: $\varepsilon_\infty = 5.3$, $\varepsilon_S = 80$, $\tau = 9.5$ps.
- The Perfectly Matched Layer is the same material of the external domain. The PML is an artificial layer with very high absorption that extinguishes the wave equations, so the actual material is not relevant.

Since the presence of magnetic materials is not contemplated, the value of magnetic permeability for all materials was approximated with the value of water (μ_R=1).

For solving the bio-heat equation, the thermal properties used in Pennes equation were also defined (taken from the online database of tissue properties [65]): ρ (density), k (thermal conductivity), C_P (heat capacity), ρ_B (blood density), C_B (blood heat capacity), ω_B (blood perfusion).

- Epineurium, endoneurium, nerve tissue and the dielectric spacer were supposed to have the same thermal characteristics for simplicity: ρ = 1075kg/m^3, k = 0.49W/(m·K), C_P = 3613 J/(kg·K), ρ_B = 1050 kg/m^3, C_B = 3617J/(kg·K), ω_B = 2.87·10^{-3}s^{-1} [65].
- For PDMS: ρ = 970kg/m^3, k = 0.15W/(m·K), C_P = 1460J/(kg·K) [64].
- For Water: ρ = 994kg/m^3, k = 0.62W/(m·K), C_P = 4177J/(kg·K) [65].

2.5 Step 1: EM waves, frequency domain

This physics study solves Maxwell equations in vector form. The most external boundaries are automatically defined as perfect electric conductors (PEC), but are overridden by the use of the perfectly matched layer, which attenuates the EM waves. The 12 sources are implemented with a **port** boundary condition on the inner boundary of the "antennas" (see figure 2.7). Since a port can only be defined on an external boundary, the area of the antenna is subtracted from all the other domains with a boolean difference operation, this way the inside of the antenna actually belongs to the external of the model. Every one of the 12 sources was defined with a different port, this way it is possible to regulate the port parameters individually. In particular the input **power** and **phase delay** were defined with different parameters, while all the ports have the same electric mode field (oriented on the z direction). A python script was implemented in order to calculate the phase delays for beamforming and modify the necessary COMSOL parameters.

Beamforming Algorithm

In order to focus the electromagnetic power, the individual phases of the sources need to be adjusted so that they are synchronous in the focal point. If we consider that the waves emitted by the source are plane waves, the wave equation is like eq. 1.24:

$$E(r,t) = E_0 e^{-\alpha r} cos(\omega(t-\tau) - \beta r) \tag{2.1}$$

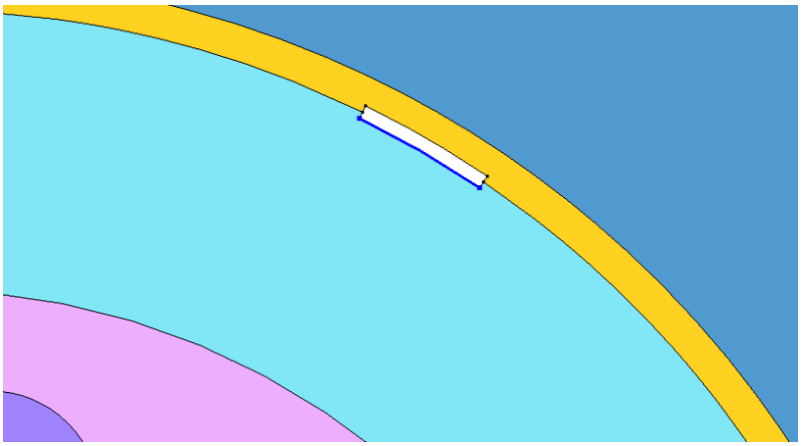

Figure 2.7: *The port boundary (highlighted in blue). The "antenna" has a width of 200μm and a thickness of 20μm*

For the moment we can ignore the contribute of the attenuation term $e^{-\alpha r}$. In the sinusoidal part, r is the distance of a point in space from the source, β is the phase constant, ω is the angular frequency, t is an instant in time and τ the time delay of the wave, which is our desired output. If we consider a focal point at a distance $r_i = d_i$ from the source, the argument of the cosine $\beta d_i - \omega(t - \tau_i)$ needs to be equal for every source in order to obtain constructive interference. Considering the maximum value of the cosine, we equal the argument to 0:

$$\omega(t - \tau_i) - \beta d_i = 0$$
$$(t - \tau_i) = -\frac{\beta}{\omega} d_i$$

Now we need to calculate the distance d_i. If the sources lay on a circumference of radius R, it is more convenient to express the coordinate of the sources in the XY plane as a function of the angle θ_i (measured from the positive y axis):

$$\begin{cases} x_{Si} = R \cdot sin\theta_i \\ y_{Si} = R \cdot cos\theta_i \end{cases}$$

the distance of the focal point of coordinates (x_F,y_F) from a source is:

$$d_i = \sqrt{(x_{Si} - x_F)^2 + (y_{Si} - y_F)^2} = \sqrt{(Rsin\theta_i - x_F)^2 + (Rcos\theta_i - y_F)^2} \tag{2.2}$$

The final equation is:

$$(t - \tau_i) = \frac{\beta}{\omega}\sqrt{(Rsin\theta_i - x_F)^2 + (Rcos\theta_i - y_F)^2} \tag{2.3}$$

By fixing an instant in time, for example t = 0, the value of τ_i can be calculated, knowing the radius, the angular position of the source and the coordinates of the

focal point. Since it is a time delay, it should be converted to a phase delay for use in COMSOL:

$$\varphi_i = \tau_i \cdot 2\pi f$$

2.6 Step 2: Bio-heat transfer

This physics study solves Pennes equation. The external boundaries are automatically defined as thermal insulators. Other boundary conditions include the initial values (set at 37°C for all the geometry) and the biological tissue, which defines the domains where the bioheat equation is valid and allows to set the parameters for blood flow (ρ_B, C_B, ω_B, T_0) and metabolic heat generation, which for this study was considered negligible (q_M = 0). It also allows to define a thickness d_Z (in 2D geometry) over which volumetric quantities are calculated. In this model d_Z was set to 1mm. A *heat source* boundary condition was added to the nerve, dielectric spacer and substrate domains which takes the total EM power dissipation density calculated in the step 1 (section 2.5) as a heat source q_S.
The study is time dependent, and is computed for 100ms in time steps of 1ms. Since we are interested in a fast temperature transient some simplifications were made:

- The effect of the blood flow was neglected, since it acts on a bigger time scale (ω_B = 0)
- The metabolic heat was neglected for the same reason (q_M = 0)
- The heat conduction is initially negligible since there is no temperature gradient (∇T = 0).

This way Pennes equation is simplified to:

$$\rho C_p \frac{dT}{dt} = q_S$$

The source term is given by the electromagnetic power density, so we can write:

$$\rho C_p \frac{dT}{dt} = \frac{1}{2}\sigma |E|^2$$

or, dividing everything by ρ and expressing it in function of the specific absorption ratio (SAR):

$$C_P \frac{dT}{dt} = \text{SAR}$$

For a discrete interval of time, we can integrate and pass from a derivative to a difference:

$$C_P \frac{\Delta T}{\Delta t} = \text{SAR}$$

By fixing one of the three variables (ΔT, Δt and SAR), a relation between the other two can be defined. In this study, a temperature increase of 1°C was considered. The relation between the irradiation time and the necessary SAR is then obtained (figure 2.8) and it shows an inverse proportionality. Since our study has a duration of 100ms, a SAR value of around 36kW/kg is necessary to cause a heating of one degree Celsius.

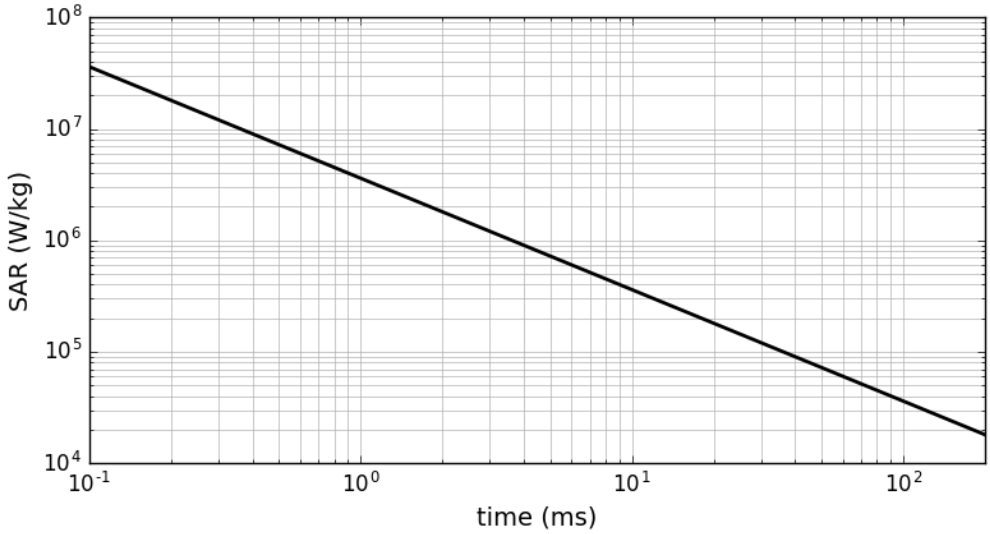

Figure 2.8: *The relationship between SAR and exposure time to obtain a temperature increase of 1°C (in logarithmic scale). At 1ms the SAR is more than 3MW/kg, at 100ms is around 36kW/kg and at 200ms is around 18kW/kg.*

Chapter 3

Results

3.1 Reference value and setup

For the following evaluations, unless stated otherwise, the average SAR value over the **fascicle n.1** was considered as a reference value. The numbering of the fascicles is showed in figure 3.1. In the homogeneous Gabriel model the same subdivision in fascicles is present in order to calculate reference values (such as fascicle average), but the whole nerve is composed by a single material.

All simulations were done at three MMW frequencies to investigate its effects:

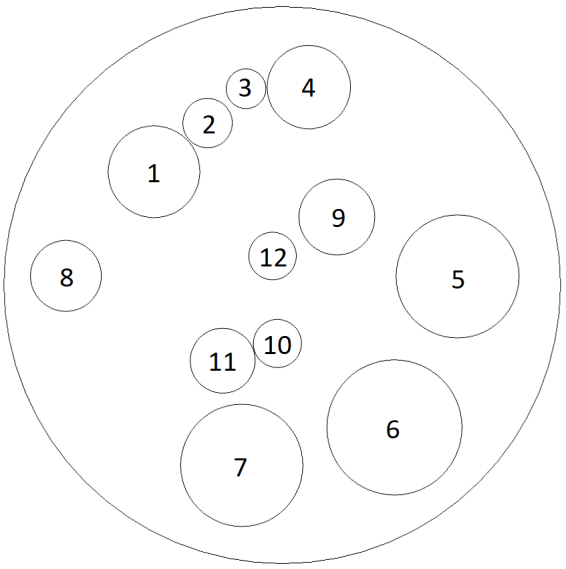

Figure 3.1: *Numbering of the nerve fascicles. The fascicle n.1 is used as a reference in the following simulations unless indicated otherwise. Fascicles 1-8 are superficial, while fascicles 9-12 are deep.*

35GHz, 61.2GHz and 122.5GHz. The first two frequencies were chosen among the MMW frequencies commonly used in therapy while the third was chosen to include a higher frequency. Two of the frequencies (61.2GHz and 122.5GHz) also belong to the ISM (Industrial, Scientifical and Medical) band. The other criteria used in the selection of the frequencies are the *skin depth* and the *wavelength*:

- For the upper frequency limit a wave that reached at least all the superficial fascicles was desired, so the position of the centres of fascicles 1-8 was measured and the maximum depth was found to be 0.4mm. The ISM frequency 122.5GHz was ideal for that purpose (δ = 0.42mm).
- The resolution of a wave is proportional to $\lambda/2$, so three frequencies with equally spaced wavelengths were chosen among the MMW frequencies found in literature.

The values of $\lambda/2$ and δ are reported in table 3.1 for some relevant frequencies. The time dependant simulations to compute the EM heating all have a duration of 100ms, unless it is indicated differently.
For determining the activation of a fascicle, the following criterion was adopted: If the minimum temperature inside a fascicle is higher than 0.5 times the maximum temperature of the whole nerve, it is considered **active**. If the average temperature of a fascicle is higher than 0.5 times the maximum temperature of the whole nerve, it is considered **partially active**. In the following figures reporting the temperature maps of the nerve, the active fascicles are represented with a *blue border*, while partially active fascicles are represented with a *dashed blue border*.

f(GHz)	$\lambda/2$	δ
35.0	**1.24mm**	**0.97mm**
42.2	1.10mm	0.82mm
61.2	**0.86mm**	**0.62mm**
78.0	0.73mm	0.53mm
122.5	**0.51mm**	**0.42mm**
140.0	0.46mm	0.40mm

Table 3.1: *Values of half-wavelength ($\lambda/2$) and skin depth (δ) for some relevant MMW frequencies. In bold are the frequencies investigated in this study.*

3.2 Gabriel model vs anatomic model

The fields in the homogeneous Gabriel model and the anatomical model were compared to verify the presence of reflections caused by the difference in dielectric constant between epineurium and endoneurium. The EM power was focused

on the center of the fascicle 1 (superficial) and on the center of the nerve (deep). All 12 sources were activated with a total input power of 100mW. The simulation was done at all three frequencies, with a dielectric spacer of thickness $\lambda/2$. The results at 61.2GHz are shown in figures 3.2 and 3.3 as representative of the data, where the SAR values and temperature increase are represented with a color map.
A first observation is that the SAR value inside the fascicles in the anatomical model is higher than in the surrounding tissue, because of the higher conductivity of the endoneurium. This causes a slight distortion in the temperature distribution with respect to the Gabriel model, as the fascicles heat up faster. The effect is more evident in figure 3.3 as the perfectly circular isothermal lines in the homogeneous model are distorted in the anatomic model.

3.3 Superficial vs deep focusing

The ability of the system to focus at two different depths was evaluated. All twelve sources were activated with a total power of 100mW. The focal point was set to the centres of the fascicles n.2 (superficial) and n.12 (deep).

- Superficial focus: (-0.28, 0.6)mm
- Deep focus: (-0.04, 0.11)mm

The simulations was repeated for all three frequencies on the anatomic model, with a matching layer of thickness $\lambda/2$. The average SAR (figure 3.4) and average temperature increase at 100ms (figure 3.5) was calculated in all the fascicles at both depth and compared. It can be seen that for deep focusing the selectivity is better at lower frequencies, as at high frequency the average SAR of the external fascicles becomes comparable or even higher than the average SAR of the focused spot. By contrast, for superficial focusing at higher frequency the selectivity becomes better as the average SAR on the focused spot becomes higher than the neighbouring ones. Looking at the average temperature plots the results are similar but less accentuated, as the heat is distributed more homogeneously by heat conduction.
The SAR and temperature plots were rendered with a color map and are presented (figures 3.6 - 3.7). It can be seen how the increase in temperature is greater at high frequency in both superficial and deep focusing. It can also be seen how the focused spot becomes smaller with increasing frequency since the wavelength of the EM waves also gets smaller, however this effect is less evident in the case of deep focusing as the attenuation also increases with the frequency and it is shadowed by the increase in temperature of the fascicles on the surface. Another aspect of interest is that the power and the consequent temperature increase are

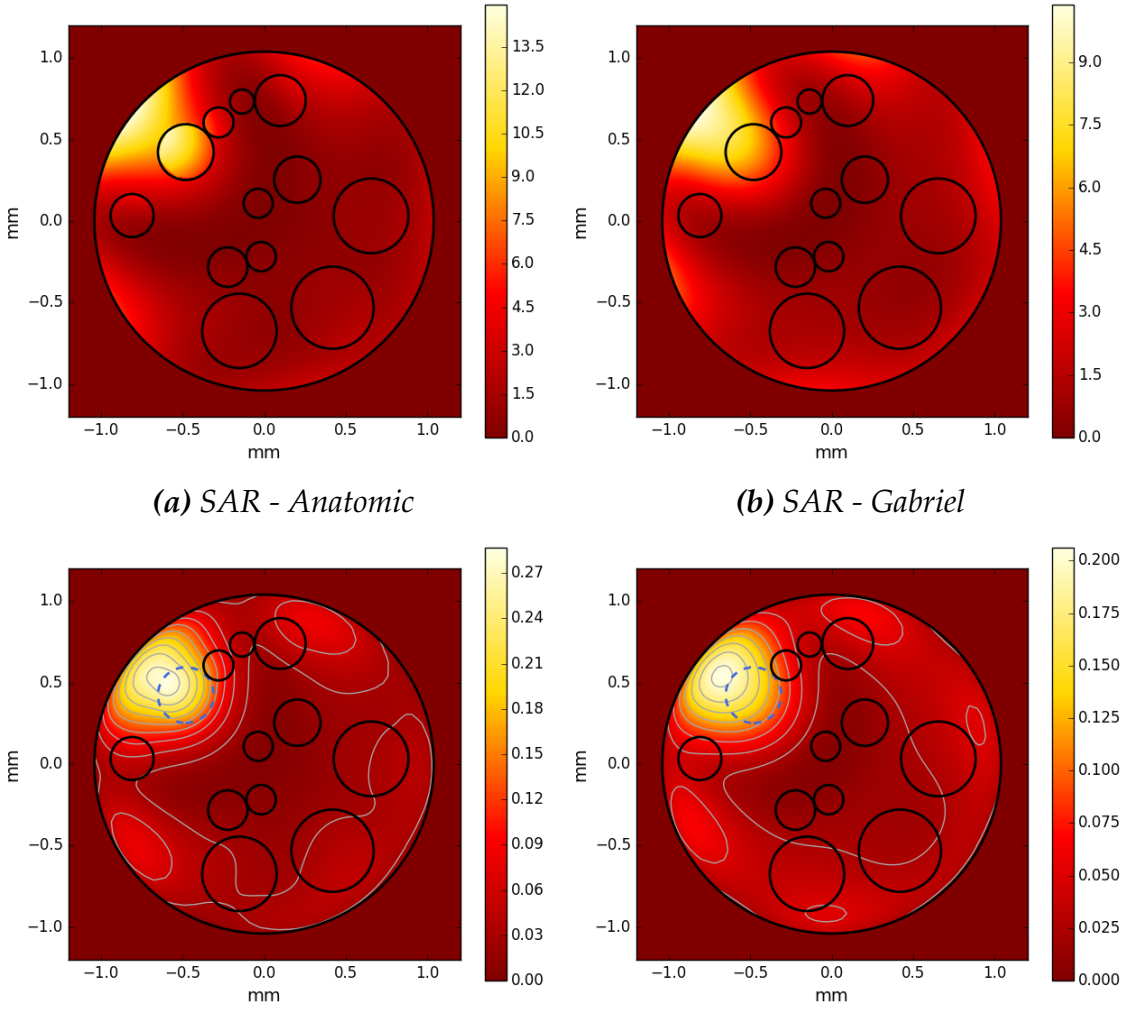

(a) *SAR - Anatomic*

(b) *SAR - Gabriel*

(c) *ΔT - Anatomic*

(d) *ΔT - Gabriel*

Figure 3.2: *Comparison of the SAR and temperature increase between the anatomical model (3.2a,3.2c) and the homogeneous Gabriel model (3.2b, 3.2d) with focusing on fascicle 1. The colorbar units are in W/kg for the SAR and °C for the temperature. The grey curves are isothermal lines. The active fascicles are represented with a blue border, the partially active fascicles are represented with a dashed blue border.*

higher when focusing near the surface because of the attenuation of the tissues, so this will be the primary application investigated.

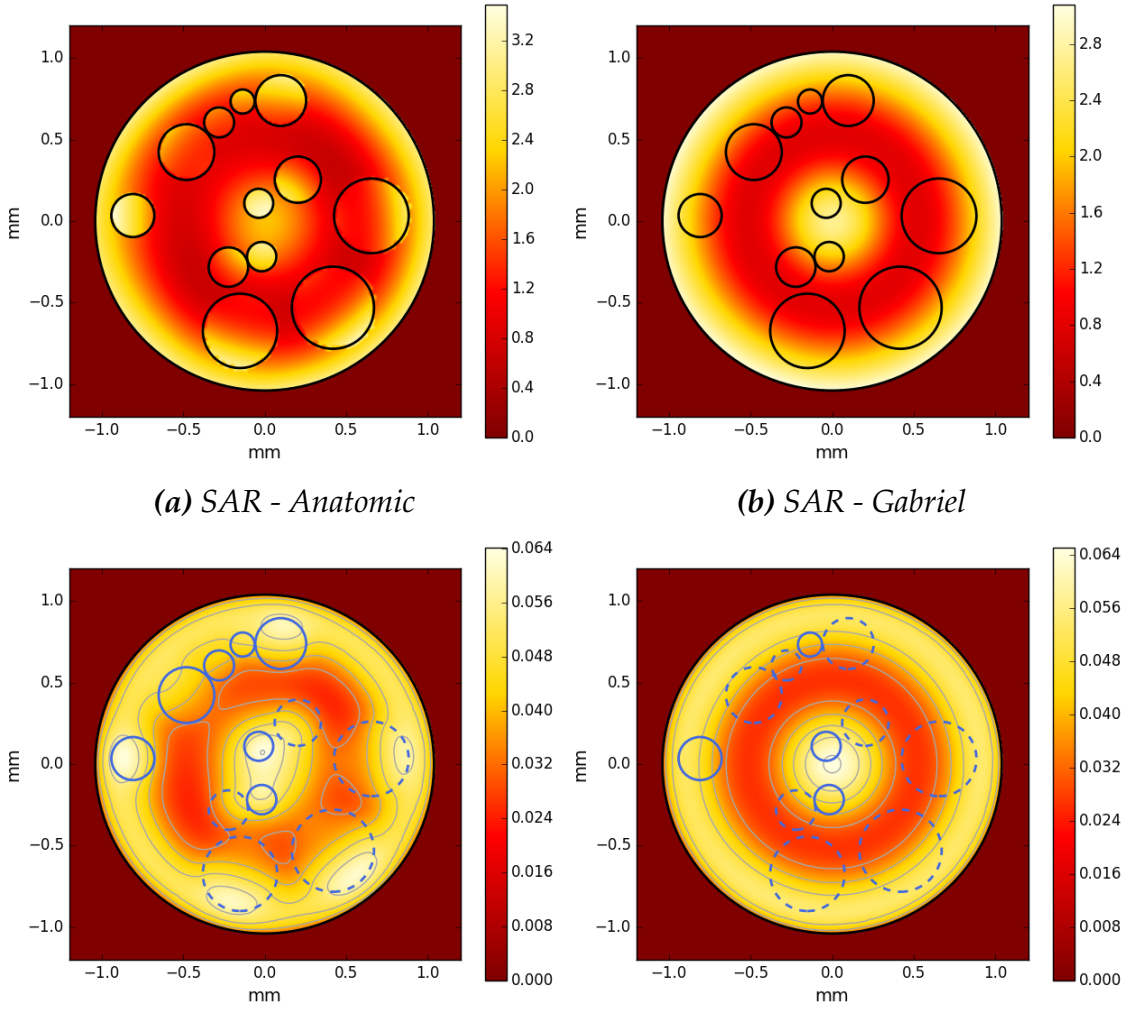

(a) *SAR - Anatomic*

(b) *SAR - Gabriel*

(c) *ΔT - Anatomic*

(d) *ΔT - Gabriel*

Figure 3.3: *Comparison of the SAR and temperature increase between the anatomical model (3.3a,3.3c) and the homogeneous Gabriel model (3.3b, 3.3d) with focusing on the center. The colorbar units are in W/kg for the SAR and °C for the temperature. The grey curves are isothermal lines. The active fascicles are represented with a blue border, the partially active fascicles are represented with a dashed blue border.*

3.4 Optimal number of active sources

When the focal point is superficial, the contribution of the farthest sources might not be actually significant. This effect should be more pronounced at higher frequencies, where the attenuation is higher. The ideal number of EM sources to activate simultaneously was determined by choosing the solution that gave the

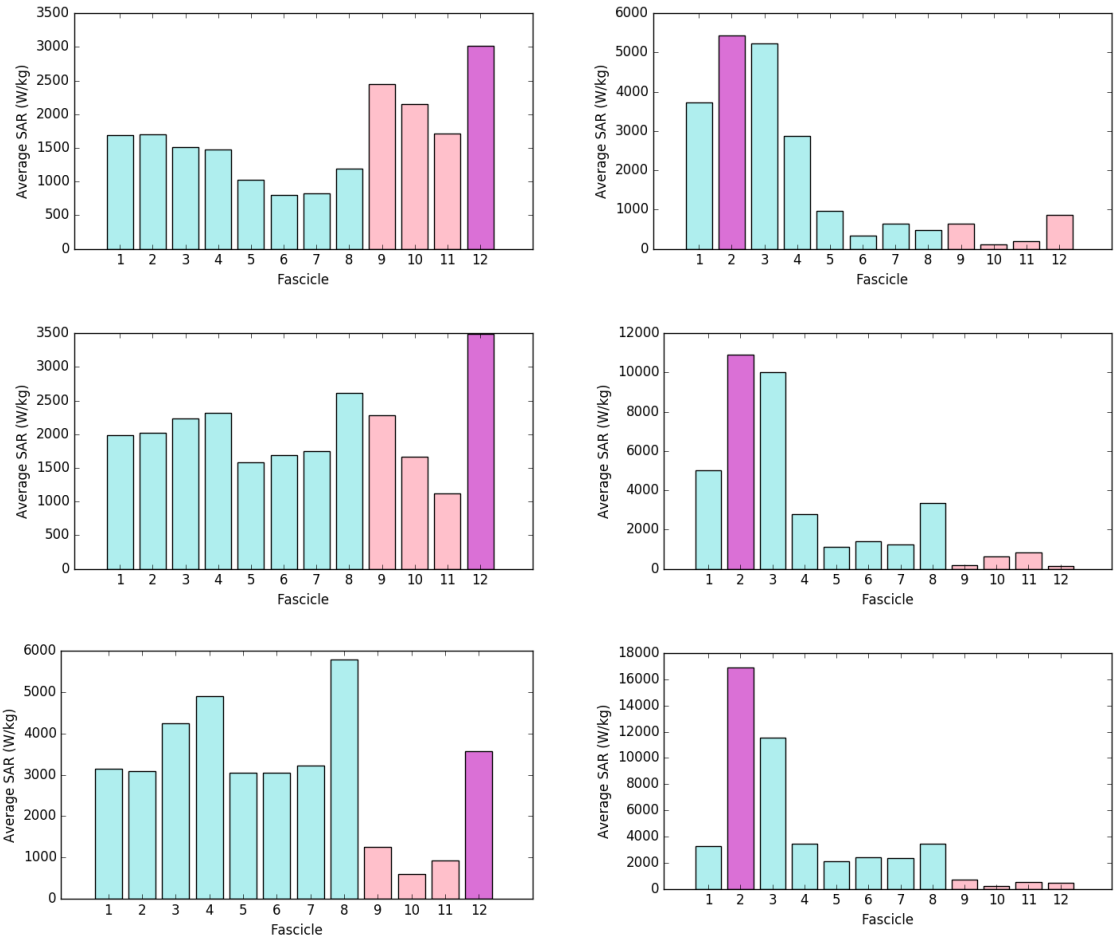

Figure 3.4: *Bar plots of the average SAR inside the 12 fascicles. Fascicles 1-8 are superficial, 9-12 are deep. On the left column the focal point is centred on the fascicle n.12 (deep, in purple), on the right column the focal point is centred on the fascicle n.2 (superficial, in purple). The values on the first row are obtained at 35GHz, on the second row at 61.2GHz and on the third row at 122.5GHz.*

highest average SAR on the reference fascicle (n.1), where the EM waves are focused. The simulation was done at all the three frequencies, with a dielectric spacer of thickness $\lambda/2$ and a total power of 100mW was divided by the number of active sources. They were chosen with the criterion that the N sources closest to the focal point would be active. The beamforming algorithm of section 2.5 was used to calculate the phase shifts in order to focus the EM waves in a focal point close to the reference fascicle center (x_F = -0.5mm, y_F = 0.4mm). The results are compared in the graphs (figure 3.8).
We can observe a decrease in the number of sources that allows the highest power

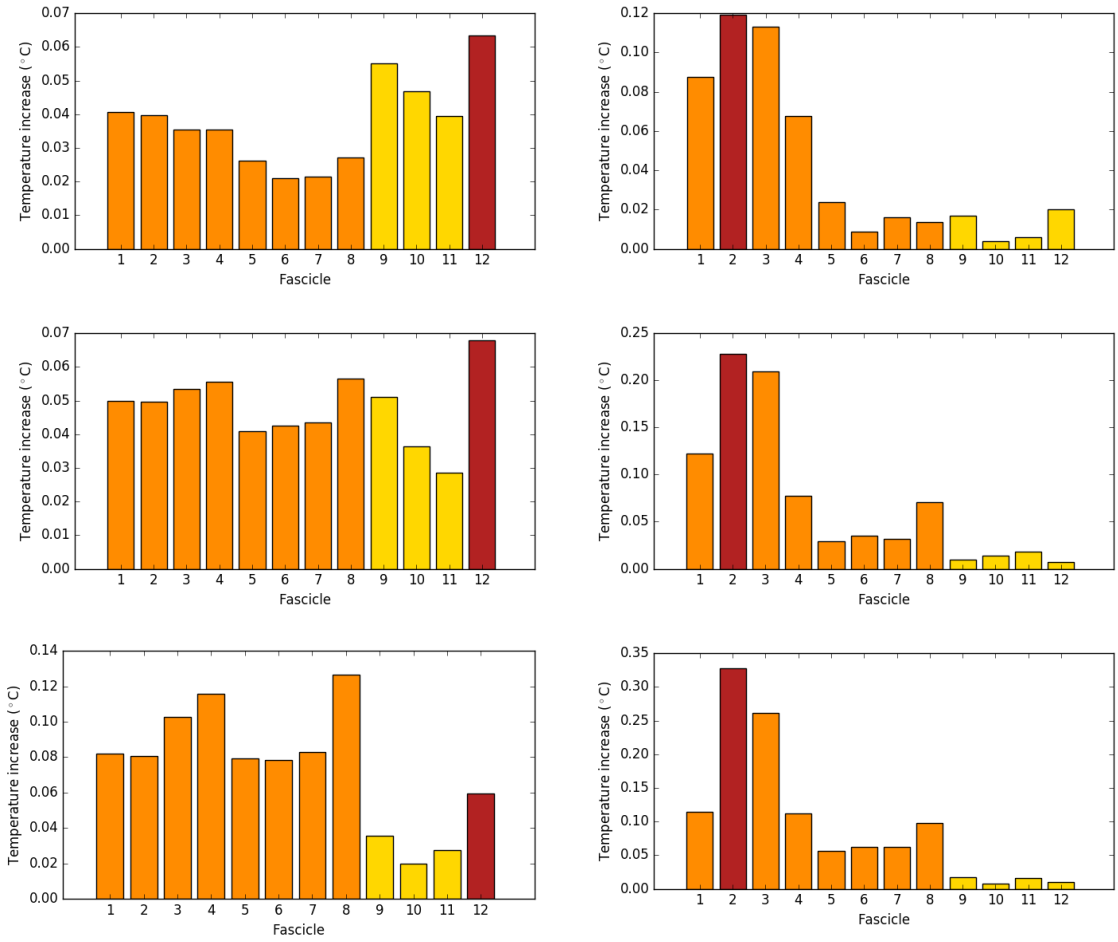

Figure 3.5: *Bar plots of the average ΔT at 100ms inside the 12 fascicles. Fascicles 1-8 are superficial, 9-12 are deep. On the left column the focal point is centred on the fascicle n.12 (deep, in red), on the right column the focal point is centred on the fascicle n.2 (superficial, in red). The values on the first row are obtained at 35GHz, on the second row at 61.2GHz and on the third row at 122.5GHz.*

concentration going up with the frequency, from 8-10 at 35GHz, to 6-10 at 61.2GHz, to 4-6 at 122.5GHz. This is consistent with the increase of the attenuation with the frequency as the power contribution of the farther sources is significantly lower. The minimum number of active sources needed to achieve the maximum SAR was determined as ideal, as less power is dissipated on the regions of the nerve far from the focal point (**N = 8 at 35GHz, N = 6 at 61.2GHz and N = 4 at 122.5GHz**).

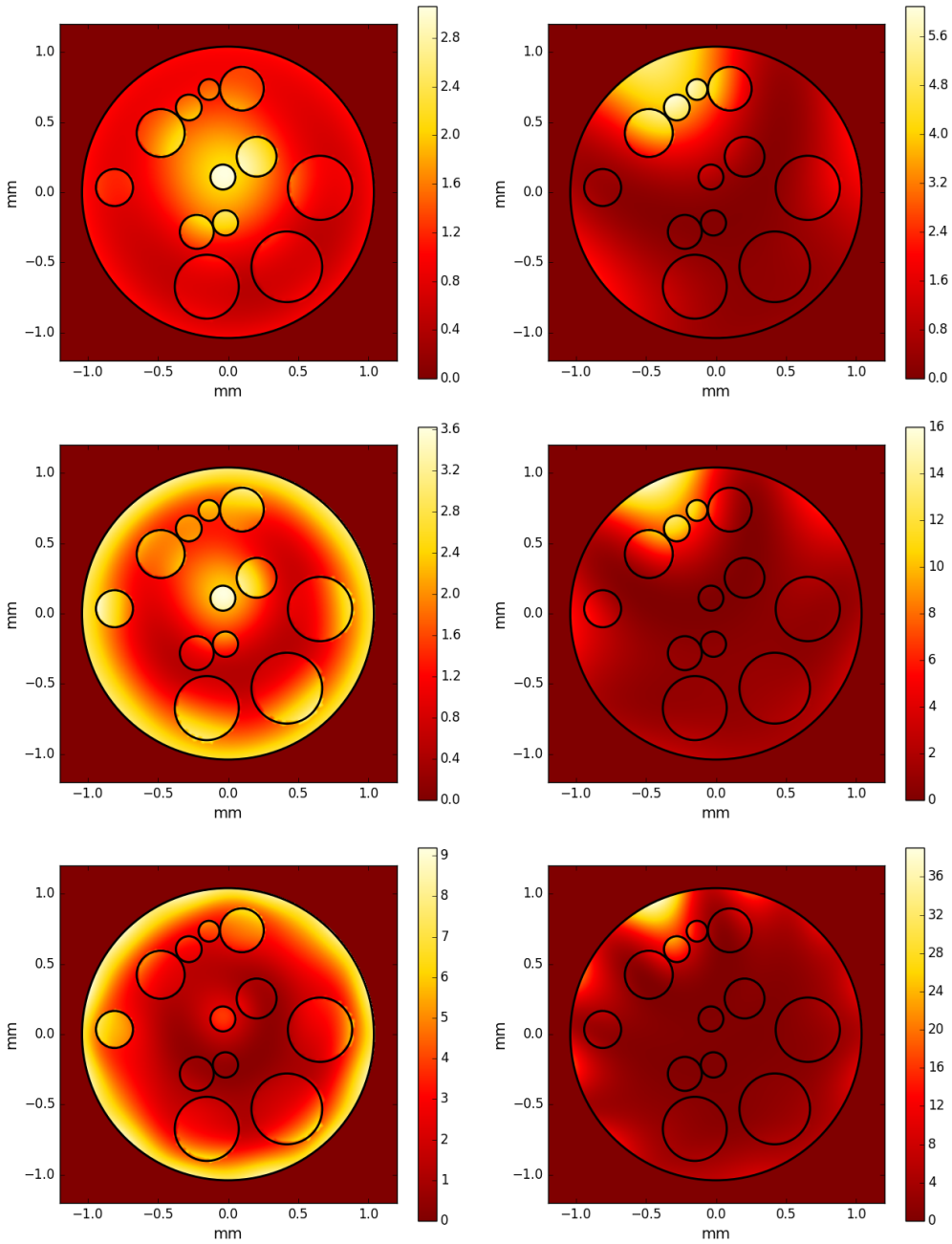

Figure 3.6: *Color map of the SAR with deep focusing (left column) and superficial focusing (right column). The frequency is 35GHz in the first row, 61.2GHz in the second row and 122.5 GHz in the third row. The color bars are in W/kg. It can be seen that focusing the EM power in deep fascicles works better at the low frequency where the attenuation is lower, but there is a higher power transfer at high frequency.*

3.5 Dielectric spacer thickness

The influence of the dielectric spacer on the power transfer was investigated. With a total input power of 100mW, using the number of sources that allowed the maximum power transfer, determined in section 3.4, a simulation was run for different dielectric spacer thickness. The best value was expected to be around $\lambda/2$, so different multiples of $50\mu m$ around that value were used. A simulation with no dielectric spacer was also done to use as a reference, in order to see if the introduction of the dielectric spacer does actually improve the power transfer or not. The focal point was centred on the fascicle n.1 and the average SAR was computed as a reference value. The simulation was repeated at 35GHz, 61.2GHz and 122.5GHz. The results are showed in the graphs (figure 3.9), with the horizontal line being the average SAR computed on the fascicle n.1 with no dielectric spacer around the nerve.
It can be seen that for all frequencies there is an improvement in the performance with respect to not using a dielectric spacer (more than 15%). The ideal thickness of the spacer at each frequency is then determined as the value that gives the maximum power (**1.1mm at 35GHz, 0.7mm at 61.2GHz and 0.4mm at 122.5GHz**). All these values are slightly smaller than half wavelength.

3.6 Extended time

With the investigated power level of 100mW, a simulation time of 100ms is not enough to obtain a significant heating, especially at lower frequencies. In figure 3.10 is shown the evolution in time of the average temperature inside fascicle 1 at the three frequencies, with the optimal parameters determined in sections 3.4 and 3.5. The relation is almost linear and the heating rate is also directly proportional to the frequency. This is consistent with the approximation made to Pennes equation in section 2.6:

$$C_P \frac{dT}{dt} = SAR$$

The equation gives as a solution a linear relation between T and t if we assume the SAR to be independent from the time, which is true if the EM sources reach the stationary state in much less time than the thermal transient (10-100ms).
Extending the simulation time should allow to obtain a greater increase in temperature. In this case the approximations that we made for the initial transient (negligible contributions of the blood flow and thermal diffusion) are not valid any more, so we set a value of $\omega_B = 2.87 \cdot 10^{-3}\text{s}^{-1}$ for all biological tissues (value taken from [65]). Increasing the simulation time to 10s, the tendency of the curves

becomes less linear (figure 3.11) because of the slower contributions of the thermal diffusion ($\nabla \cdot k\nabla T$) and blood flow ($-\omega_B \rho_B C_B (T - T_0)$). The time required to heat the fascicle 1 by 1°C is 1.2s at 35GHz, 400ms at 61.2GHz and 150ms at 122.5GHz.
The temperature maps obtained after 1s, 5s and 10s of simulation at 61.2GHz are showed in figure 3.12 as representative of the data. From the fascicle activations and the isothermal curves it can be seen that the heated portion grows in size because of thermal conduction, so incrementing the exposition times implies a reduction in selectivity.

3.7 Increase in power

Since the heating rate with 100mW input power is too low for our application (Irradiation times going from 1.2s at 35 GHz to 150ms at 122.5GHz are required to cause a temperature raise of 1° C), simulations were done at 500mW, 1W and 5W in order to reduce the irradiation time and examine the dependence of the heating rate from the input power. Ideally, in order to have stimulation times comparable with laser stimulation (10 °C in 1-10ms [50]) a heating rate of 1000 - 10000 °C/s is needed. Since the heating during the initial transient is linear, an average heating rate over the simulation time (100ms) was calculated as

$$\frac{T_{final} - T_{initial}}{100ms}$$

The simulation were done at all three frequencies on the anatomical model with the optimal number of sources and dielectric spacer thickness found in sections 3.4 and 3.5, with a duration of 100ms. The EM power was focused on the center of the fascicle 1 and the average temperature of the fascicle was used as a reference value. In figure 3.14 the evolution of the average temperature in time with an input power of 500mW, 1W and 5W is showed. The trend is almost linear, just like with a 100mW power input (figure 3.10), but the heating rate is higher. All the values are reported in table 3.2 and plotted in figure 3.13. It can be seen that the heating rate is proportional to the frequency and it increases linearly with the input power so, theoretically, any desired value can be obtained by using an appropriate level of input power. With a power of 5W, the heating rate is still far from the one obtained in laser stimulation, but a relevant increase of temperature can still be obtained using a 122.5GHz source (∼3.3°C in 10ms).

	Input power			
frequency	100mW	500mW	1W	5W
35GHz	1.6°C/s	8°C/s	16°C/s	80°C/s
61.2GHz	3.2°C/s	16°C/s	32°C/s	160°C/s
122.1GHz	6.7°C/s	33.6°C/s	67°C/s	335.8°C/s

Table 3.2: *Average heating rates of fascicle 1 over 100ms at three different frequencies and four total input powers.*

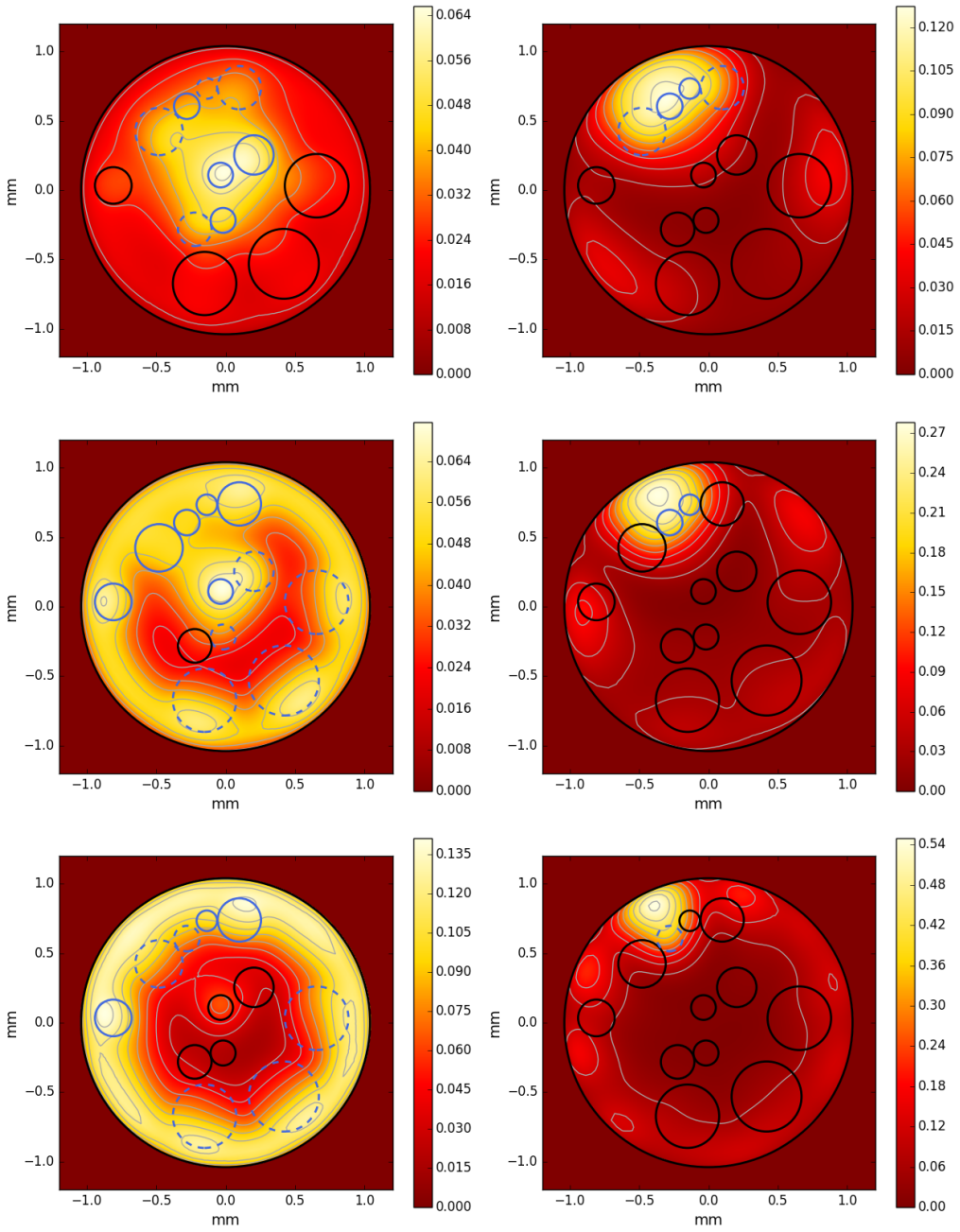

Figure 3.7: *Color map of the temperature increase (with respect to 37°C) with deep focusing (left column) and superficial focusing (right column). The frequency is 35GHz in the first row, 61.2GHz in the second row and 122.5 GHz in the third row. The color bars are in degree Celsius, the grey curves are isothermal lines. The active fascicles are represented with a blue border, the partially active fascicles are represented with a dashed blue border. At 61.2GHz the ΔT at the center is comparable with the one on the surface, while at 122.5GHz the ΔT on the surface is twice with respect to the center.*

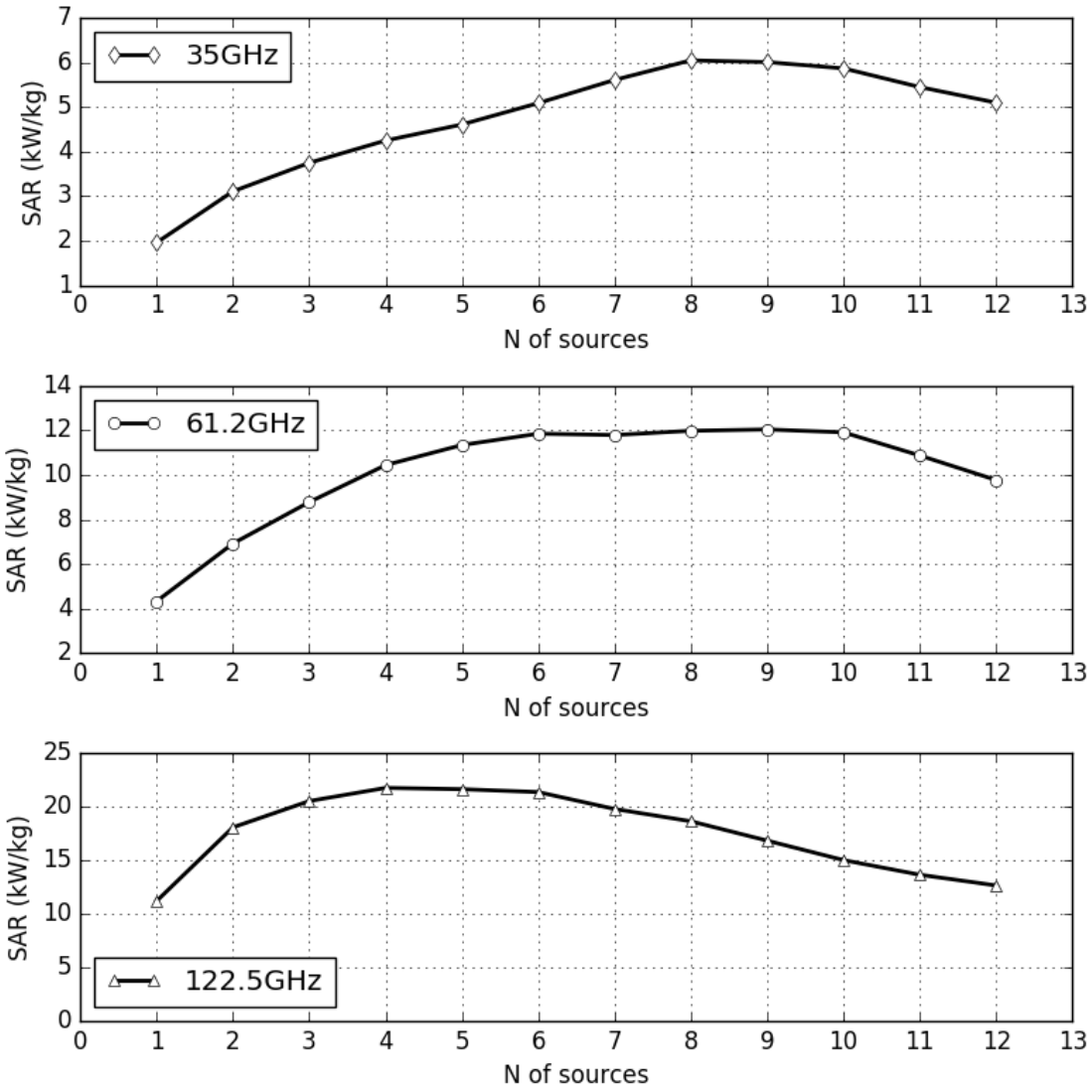

Figure 3.8: *Relation between the number of active sources and the average SAR over the fascicle 1, with a total input power of 100mW divided by the number of active sources (N) and focused on the fascicle center. The simulation was done at three frequencies, with a dielectric spacer of thickness $\lambda/2$.*

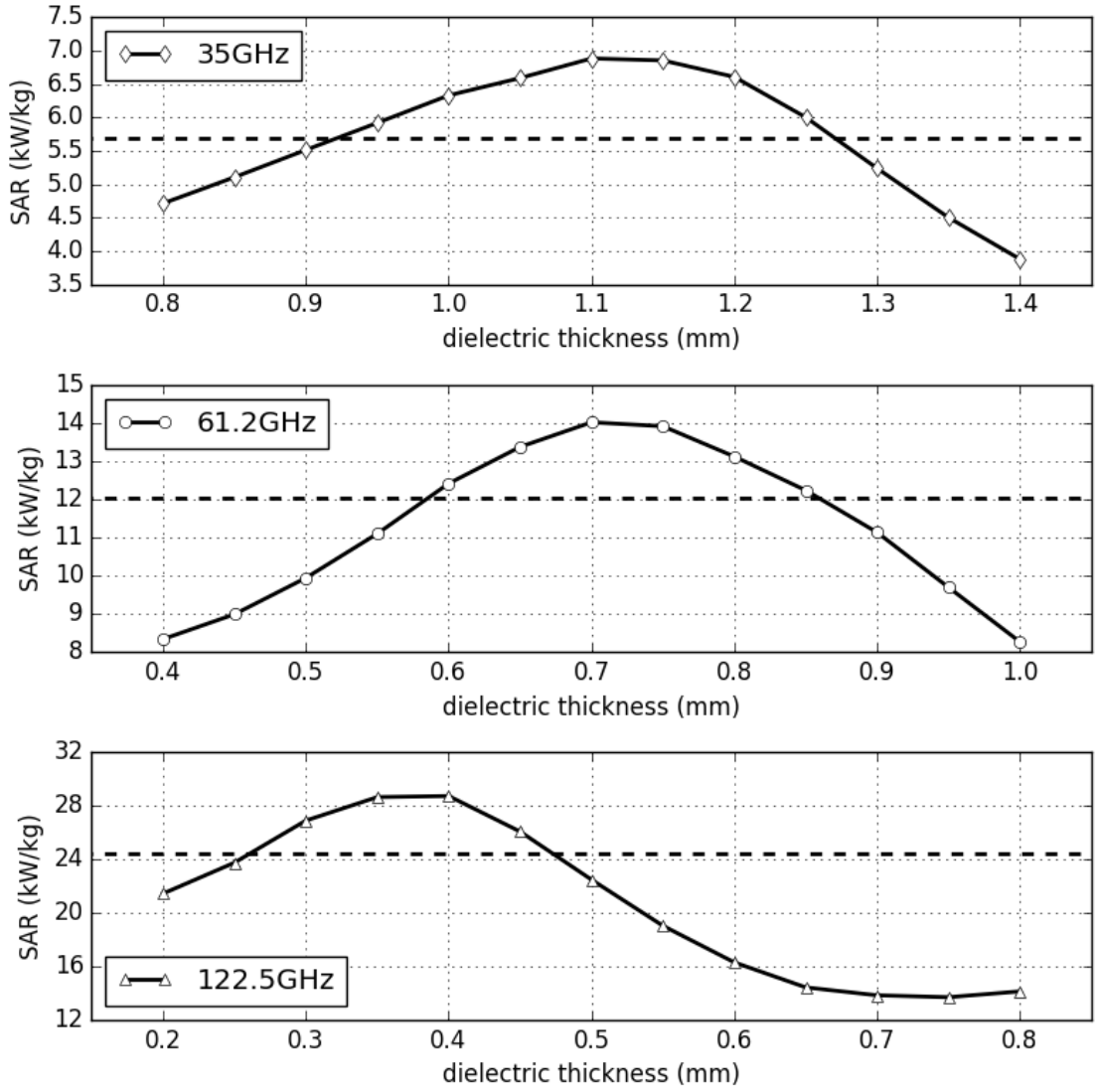

Figure 3.9: *Relation between the dielectric spacer thickness and the average SAR over the fascicle n.1, with a total input power of 100mW divided between the optimal number of active sources at each frequency (8 at 35GHz, 6 at 61.2GHz, 4 at 122.5GHz). The horizontal dashed line represents the same value calculated with no dielectric spacer and is used as a reference.*

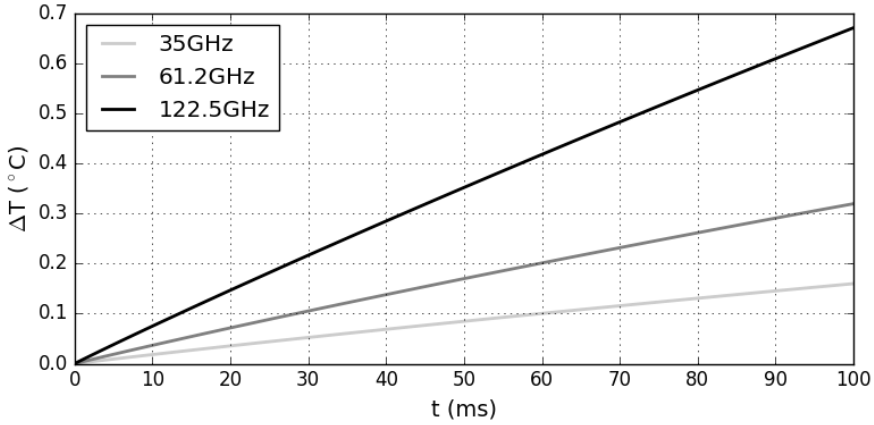

Figure 3.10: *Average increase of temperature inside the fascicle 1 for a simulation of length 100ms at three different frequencies. The trend is almost linear as the only non negligible contribution comes from the SAR (which is constant on average).*

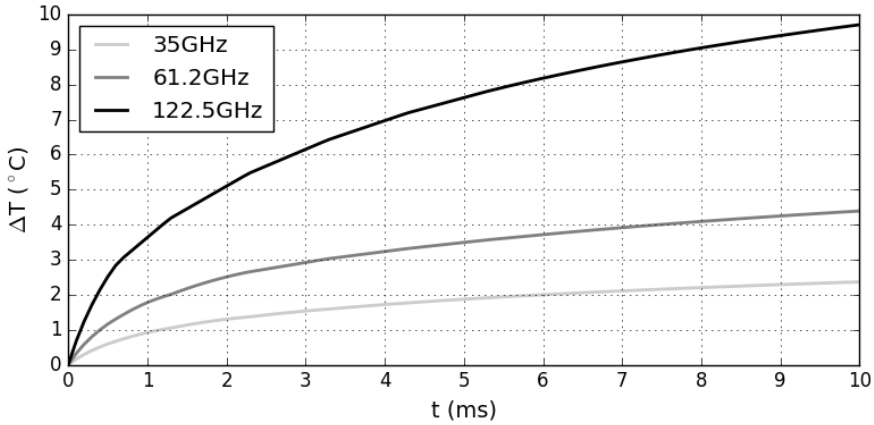

Figure 3.11: *Average increase of temperature inside the fascicle 1 for a simulation of duration 10s at three different frequencies. The loss of linearity with respect to the initial transient of 100ms (figure 3.10) is to be attributed to the conduction of heat and blood flow, which act on a longer time scale.*

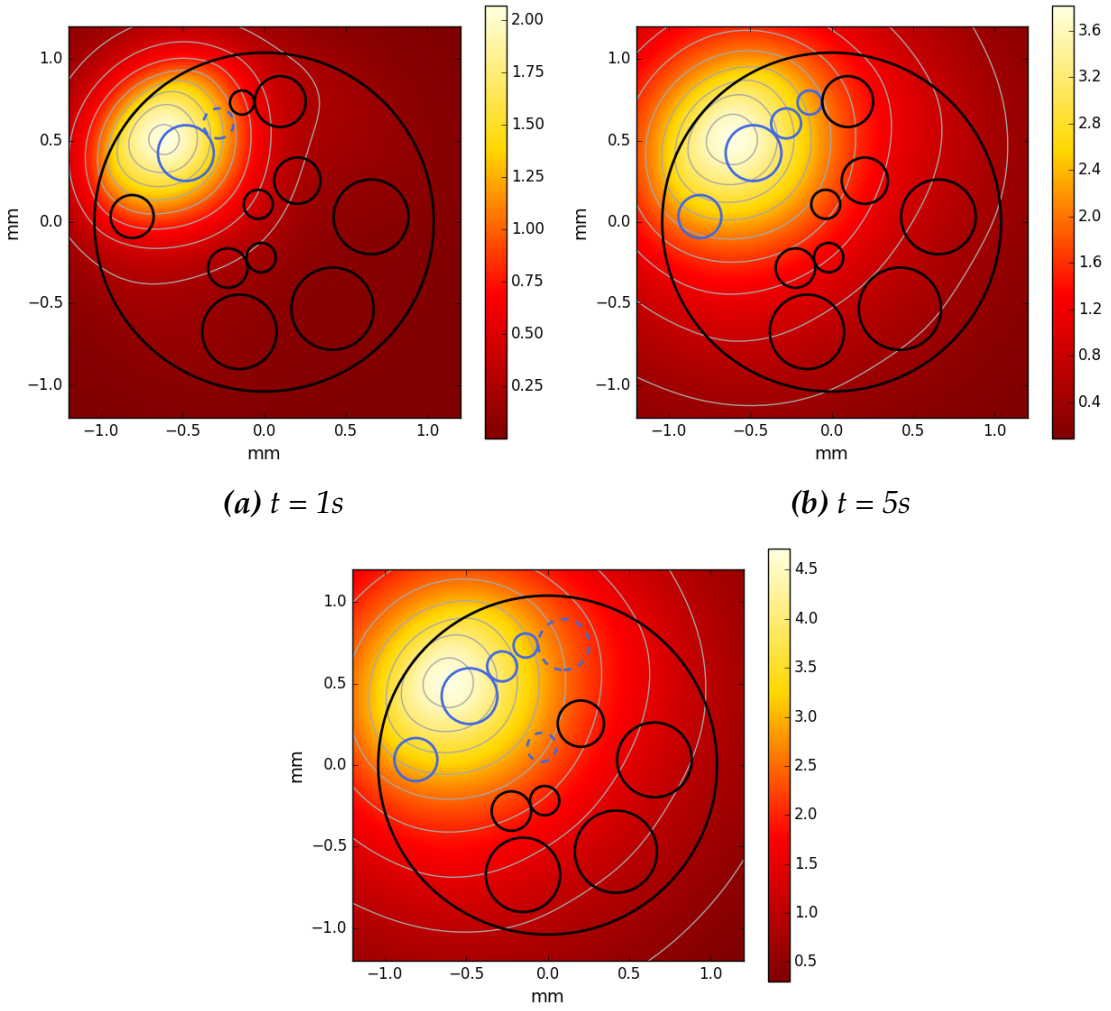

(a) *t = 1s*

(b) *t = 5s*

(c) *t = 10s*

Figure 3.12: *Temperature map of the nerve with a total power of 100mW focused on fascicle 1 at 61.2GHz, for a stimulation time of 1s (3.12a), 5s (3.12b), 10s (3.12c). The grey curves are isothermal lines. The active fascicles are represented with a blue border, the partially active fascicles are represented with a dashed blue border.*

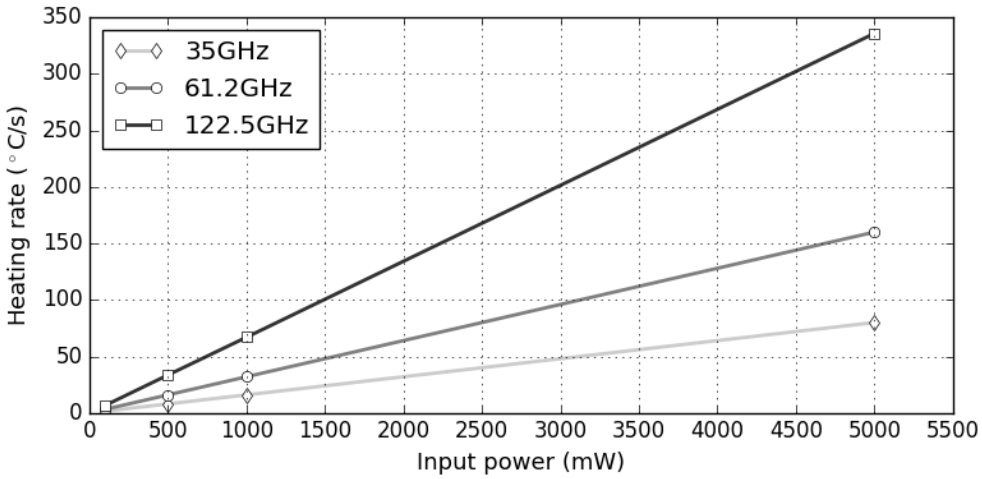

Figure 3.13: *Graph of the values in table 3.2. It is shown that the relation between the heating rate and the input power is linear.*

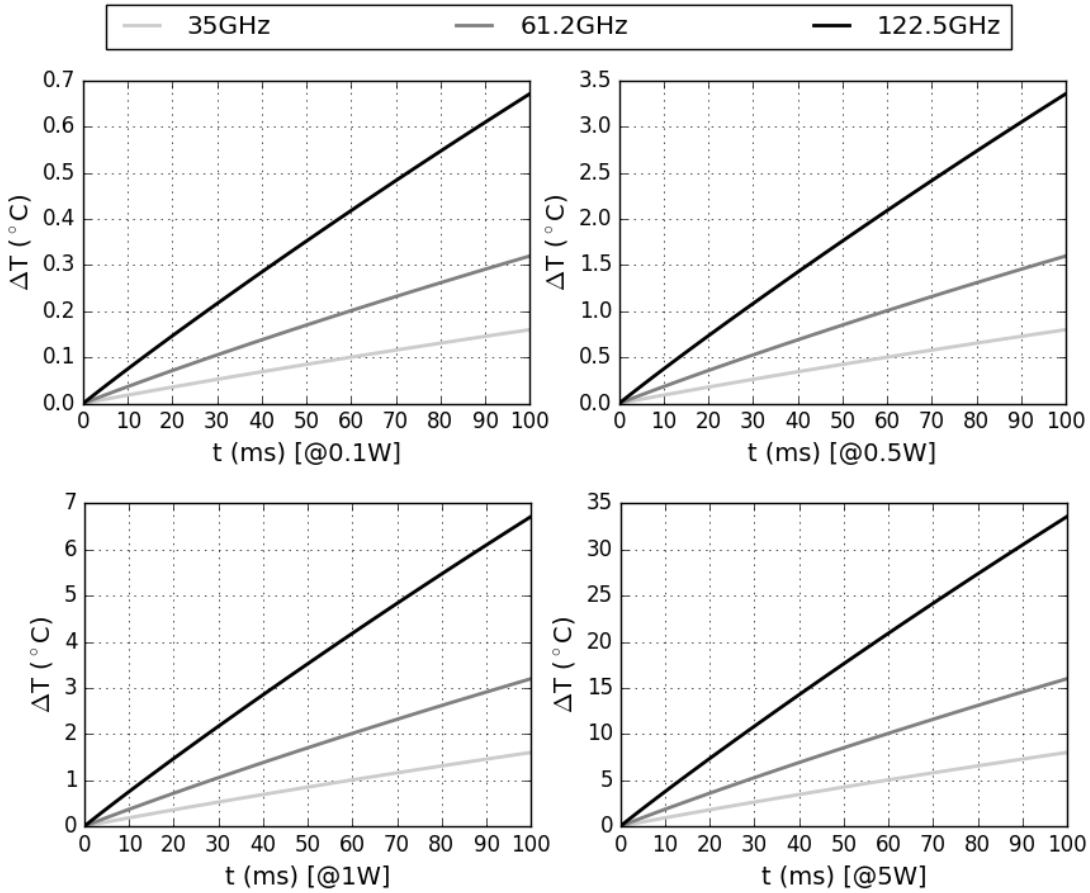

Figure 3.14: *The time evolution of the average temperature on fascicle 1 with increasing power levels (in square brackets). The EM waves are focused on the center of fascicle 1 and the ideal simulation parameter determined in section 3.4, 3.5 for each frequency were used. The time evolution in the transitory is the same, but the heat rate increases linearly with the power.*

Chapter 4

Discussion

The proposed device for electromagnetical heating with millimetre waves for neural stimulation was investigated. Firstly a more accurate nerve model was developed which accounts for two different tissues contained inside a nerve (section 2.2): the epineurium (mostly connective tissue) and the endoneurium (which contains the axons). The difference of conductivity between the two tissues caused by the presence of neurons inside the endoneurium could be an advantage for this application as the SAR inside the fascicles is higher than the SAR in the surrounding epineurium (as can be seen in figures 3.3, 3.2), so the heating rate also should be higher inside the fascicles. On the contrary, the different dielectric constant causes reflections of the incident EM waves, so the shape of the focused spot is less regular (as can be seen in figure 3.3). The device was showed to have poor performance at focusing the EM power in deep fascicles with respect to focusing in superficial fascicles: the selectivity was good enough only at the lowest chosen frequency (35GHz) because there is less attenuation and the SAR value on the superficial fascicles is lower than at the center. However a low frequency also means less EM power (σ is directly proportional to the frequency) and a larger focused spot (λ is higher), diminishing the desired heating effect.
For this reason the principal application investigated was superficial focusing of the EM power. The ideal number of sources to be activated (section 3.4) and the adequate dielectric spacer thickness (section 3.5) were determined for each of the three frequencies.
If compared with electrical and optic stimulation, the time needed for heating the nerve using an input power of 100mW is too long (100-200ms, opposed to 1-10ms in optic stimulation and <1ms in electrical stimulation) so a higher power should be used. Simulations at power inputs of 500mW, 1W and 5W were done and the heating rate showed a linear relation with the power, meaning that the desired value could theoretically be obtained by raising the amount of power irradiated inside the system. A safety considerations should be however made: the maximum temperature increase should not be high enough to provoke irreversible

changes to the tissues (around 50°C the blood starts to coagulate and cells die in few minutes [66]). Considering a body temperature of 37°C, the stimulation parameters should be chosen in order to obtain a maximum temperature raise of 10°C (having a safety margin of 3°C). Another way to increase the heating rate could be by raising the frequency, which also showed a direct proportionality with the EM power. There might be however a frequency limit given by the filtering action of the tissues: the attenuation increases with the frequency and if it grows too much there is a risk of heating just a thin superficial layer of connective tissue, without reaching the fascicles. In section 3.1 the maximum frequency with a skin depth greater than the superficial fascicles depth was determined to be 140GHz.
Simulations were also done by maintaining an input power of 100mW and extending the simulation time to 10s, reintroducing the contribution of blood flow. This was done to see the heating capabilities of the device on prolonged irradiation at low power. This modality does not have useful applications in neurostimulation as the selectivity is worse, but it can be employed in other types of thermal treatments, like pain relief by heat blocking.
In conclusion, the proposed device is probably suitable for neurostimulation of superficial fascicles using the appropriate frequency and level of power, but it can also find use in nerve inhibition (by means of heat block [22]) for analgesic purposes.

4.1 Future work

A first study to make is about the EM sources: in this study they were modelled with EM ports, which is an idealization. A real source of EM waves should be developed and studied for this specific application, such as antennas for near field.
The beam focusing algorithm also makes use of some approximations. The propagating waves are supposed to be planar waves, while in reality there is a spreading factor $1/r$ that results in a shift of the maximum power peak with respect to the focal point [67, 68]. This effect could be accounted for in the algorithm if a greater precision is needed for some specific applications.
A long time simulation of the heat transfer after a heating pulse should be made in order to see how the heat dissipates inside the tissues, if the flexible substrate acts as a thermal insulator and to determine the relaxation time needed to return the tissue to body temperature (37°C).
Lastly, a full 3D model of the device should be designed and used for the simulations to obtain a more accurate representation of the electric field inside the

tissues. In the present study a 3D model of 1mm thickness was actually developed, but the high computation cost required did not allow to obtain a converging solution on the machine. A computer with a high amount of memory is recommended for the simulations (ideally a cluster).

Bibliography

[1] T. K. Sarkar, R. Mailloux, A. A. Oliner, M. Salazar-Palma, and D. L. Sengupta, *Maxwell, Hertz, the Maxwellians and the Early History of Electromagnetic Waves*. Wiley-IEEE Press, 2006, pp. 215–228. [Online]. Available: http://ieeexplore.ieee.org/xpl/articleDetails.jsp?arnumber=5237157

[2] N. Levanon, *Radar principles*, 1988.

[3] W. C. Jakes and D. C. Cox, Eds., *Microwave Mobile Communications*. Wiley-IEEE Press, 1994.

[4] A. Metaxas, , and R. J. Meredith, *Industrial microwave heating*. IET, 1983, no. 4.

[5] E. Seeram, *Computed Tomography: Physical Principles, Clinical Applications, and Quality Control*. Elsevier Health Sciences, 2015.

[6] J.-M. Jin, "Electromagnetics in magnetic resonance imaging," *IEEE Antennas and Propagation Magazine*, vol. 40, no. 6, pp. 7–22, December 1998.

[7] A. W. Guy, J. F. Lehmann, and J. B. Stonebridge, "Therapeutic applications of electromagnetic power," *Proceedings of the IEEE*, vol. 62, no. 1, pp. 55–75, January 1974.

[8] P. M. Van Den Berg, A. T. De Hoop, A. Segal, and N. Praagman, "A computational model of the electromagnetic heating of biological tissue with application to hyperthermic cancer therapy," *IEEE Transactions on Biomedical Engineering*, vol. BME-30, no. 12, pp. 797–805, December 1983.

[9] T. I. Usichenko and H. F. Herget, "Treatment of chronic pain with millimetre wave therapy (mwt) in patients with diffuse connective tissue diseases: a pilot case series study," *European Journal of Pain*, vol. 7, no. 3, pp. 289 – 294, 2003. [Online]. Available: http://www.sciencedirect.com/science/article/pii/S1090380102001258

[10] M. K. Logani, I. Szabo, V. Makar, A. Bhanushali, S. Alekseev, and M. C. Ziskin, "Effect of millimeter wave irradiation on tumor metastasis," *Bioelectromagnetics*, vol. 27, no. 4, pp. 258–264, 2006. [Online]. Available: http://dx.doi.org/10.1002/bem.20208

[11] A. Pakhomov and M. Murphy, "Low-intensity millimeter waves as a novel therapeutic modality," in *Digest of Technical Papers. 12th IEEE International Pulsed Power Conference. (Cat. No.99CH36358)*, vol. 1, Jun 1999, pp. 23–28.

[12] L. Kolosova, G. Akoev, V. Avelev, O. Riabchikova, and K. Babu, "Effect of low-intensity millimeter wave electromagnetic radiation on regeneration of the sciatic nerve in rats," *Bioelectromagnetics*, vol. 17, no. 1, pp. 44–47, 1996. [Online]. Available: http://dx.doi.org/10.1002/(SICI)1521-186X(1996)17:1<44::AID-BEM6>3.0.CO;2-6

[13] M. V. Matveev, A. I. Erofeev, S. G. Terekhin, P. V. Plotnikova, K. V. Vorobyov, and O. L. Vlasova, "Implantable devices for optogenetic studies and stimulation of excitable tissue," *St. Petersburg Polytechnical University Journal: Physics and Mathematics*, vol. 1, no. 3, pp. 264 – 271, 2015. [Online]. Available: http://www.sciencedirect.com/science/article/pii/S2405722315300578

[14] K. Deisseroth, "Optogenetics," *Nature methods*, vol. 8, no. 1, pp. 26–29, Jan 2011.

[15] M. Hausser, "Optogenetics: the age of light," *Nature methods*, no. 10, pp. 1012–1014, Oct 2014.

[16] T. Bécherrawy, "Maxwell's equations," in *Electromagnetism: Maxwell Equations, Wave Propagation and Emission*. John Wiley & Sons, Inc., 2013, pp. 263–282. [Online]. Available: http://dx.doi.org/10.1002/9781118562215.ch9

[17] A. A. Radzievsky *et al.*, "Peripheral neural system involvement in hypoalgesic effect of electromagnetic millimeter waves," *Life Sciences*, vol. 68, pp. 1143–1151, 2001.

[18] A. Radzievsky, O. Gordiienko, S. Alekseev, I. Szabo, A. Cowan, and M. Ziskin, "Electromagnetic millimeter wave induced hypoalgesia: Frequency dependence and involvement of endogenous opioids," *Bioelectromagnetics*, vol. 29, pp. 284–295, May 2008.

[19] S. I. Alekseev, O. V. Gordiienko, A. A. Radzievsky, and M. C. Ziskin, "Millimeter wave effects on electrical responses of the sural nerve in vivo," *Bioelectromagnetics*, vol. 31, pp. 180–190, 2010.

[20] V. Pikov, X. Arakaki, M. Harrington, S. E. Fraser, and P. H. Siegel, "Modulation of neuronal activity and plasma membrane properties with low-power millimeter waves in organotypic cortical slices," *Journal of Neural Engineering*, vol. 7, no. 4, p. 045003, 2010. [Online]. Available: http://stacks.iop.org/1741-2552/7/i=4/a=045003

[21] M. Shapiro, M. Priest, P. Siegel, and F. Benzanilla, "Thermal mechanisms of millimeter wave stimulation of excitable cells," *Biophysical Journal*, vol. 104, no. 12, pp. 2622–2628, 2013.

[22] Z. Mou, I. F. Triantis, V. M. Woods, C. Toumazou, and K. Nikolic, "A simulation study of the combined thermoelectric extracellular stimulation of the sciatic nerve of the xenopus laevis: The localized transient heat block," *IEEE transactions on biomedical engineering*, vol. 59, no. 6, pp. 1758–1769, June 2012.

[23] J. W. Valvano, *Bioheat Transfer*. John Wiley & Sons, Inc., 2006. [Online]. Available: http://dx.doi.org/10.1002/0471732877.emd015

[24] R. W. Y. Habash, R. Bansal, D. Krewski, and H. T. Alhafid, "Thermal therapy, part 1: An introduction to thermal therapy," *Critical Reviews in Biomedical Engineering*, vol. 34, no. 6, pp. 459–489, 2006.

[25] H. H. Pennes, "Analysis of tissue and arterial blood temperatures in the resting human forearm," *Journal of Applied Physiology*, vol. 85, no. 1, pp. 5–34, 1998.

[26] (2011). [Online]. Available: http://www2.highlands.edu/academics/divisions/scipe/biology/faculty/harnden/2121/notes/ans.htm

[27] J. Chawla. (2016, Jun) Peripheral nervous system anatomy. [Online]. Available: https://emedicine.medscape.com/article/1948687-overview#a2

[28] G. McKane and G. Karp, *Biology, Exploring Life. Second edition*. John Wiley & Sons Inc., Jul 1996, ch. 23.

[29] D. S. Butler, *The Sensitive Nervous System*. Noigroup Publications, 2000.

[30] A. Parent, *Carpenter's human neuroanatomy*. Williams & Wilkins, 1996.

[31] OpenStax College, *Anatomy and Physiology*. OpenStax CNX, Aug 2017. [Online]. Available: http://cnx.org/contents/14fb4ad7-39a1-4eee-ab6e-3ef2482e3e22@8.108

[32] A. Handforth, C. M. DeGiorgio, S. C. Schachter *et al.*, "Vagus nerve stimulation therapy for partial-onset seizures," *Neurology*, vol. 51, no. 1, pp. 48–55, 1998. [Online]. Available: http://n.neurology.org/content/51/1/48

[33] C. M. DeGiorgio, S. C. Schachter, A. Handforth *et al.*, "Prospective long-term study of vagus nerve stimulation for the treatment of refractory seizures," *Epilepsia*, vol. 41, no. 9, pp. 1195–1200, 2000. [Online]. Available: http://dx.doi.org/10.1111/j.1528-1157.2000.tb00325.x

[34] D. N. Rushton, "Electrical stimulation in the treatment of pain," *Disability and Rehabilitation*, vol. 24, no. 8, pp. 407–415, 2002.

[35] A. Picaza J, E. Hunter S, and W. Cannon B, "Pain suppression by peripheral nerve stimulation," *Applied Neurophysiology*, vol. 40, pp. 223–234, 1977.

[36] K. Stingl, K. U. Bartz-Schmidt, D. Besch *et al.*, "Subretinal visual implant alpha ims – clinical trial interim report," *Vision Research*, vol. 111, pp. 149 – 160, 2015.

[37] R. P. Michelson, "Electrical stimulation of the human cochlea: A preliminary report," *Archives of Otolaryngology*, vol. 93, no. 3, pp. 317–323, 1971.

[38] N. Rijkhoff, H. Wijkstra, P. Van Kerrebroeck, and F. Debruyne, "Urinary bladder control by electrical stimulation: Review of electrical stimulation techniques in spinal cord injury," *Neurourology and Urodynamics*, vol. 16, no. 1, pp. 39–53, 1997. [Online]. Available: http://dx.doi.org/10.1002/(SICI)1520-6777(1997)16:1<39::AID-NAU6>3.0.CO;2-F

[39] D. N. Rushton, "Functional electrical stimulation and rehabilitation: an hypothesis," *Medical Engineering & Physics*, vol. 25, pp. 75–78, 2003.

[40] S. C. Schachter and C. B. Saper, "Vagus nerve stimulation," *Epilepsia*, vol. 39, no. 7, pp. 677–686, 7 1998. [Online]. Available: http:https://doi.org/10.1111/j.1528-1157.1998.tb01151.x

[41] D. Guiraud, D. Andreu, S. Bonnet *et al.*, "Vagus nerve stimulation: State of the art of stimulation and recording strategies to address autonomic function neuromodulation," *Journal of Neural Engineering*, vol. 13, no. 4, p. 041002, 2016. [Online]. Available: https://hal-univ-rennes1.archives-ouvertes.fr/hal-01372361

[42] Deep Thought, "The answer to the ultimate question of life, the universe, and everything," *The Hitchhiker's guide to the Galaxy*, 1979.

[43] K. Y. Qing, M. P. Ward, and P. P. Irazoqui, "Burst-modulated waveforms optimize electrical stimuli for charge efficiency and fiber selectivity," *IEEE Transactions on Neural Systems and Rehabilitation Engineering*, vol. 23, no. 6, pp. 936–945, Nov 2015.

[44] W. M. Grill and J. T. Mortimer, "Stimulus waveforms for selective neural stimulation," *IEEE Engineering in Medicine and Biology Magazine*, vol. 14, no. 4, pp. 375–385, Jul 1995.

[45] Z. P. Fang and J. T. Mortimer, "A method to effect physiological recruitment order in electrically activated muscle," *IEEE Transactions on Biomedical Engineering*, vol. 38, no. 2, pp. 175–179, Feb 1991.

[46] J. D. Sweeney, D. A. Ksienski, and J. T. Mortimer, "A nerve cuff technique for selective excitation of peripheral nerve trunk regions," *IEEE Transactions on Biomedical Engineering*, vol. 37, no. 7, pp. 706–715, Jul 1990.

[47] C. Veraart, W. M. Grill, and J. T. Mortimer, "Selective control of muscle activation with a multipolar nerve cuff electrode," *IEEE Transactions on Biomedical Engineering*, vol. 40, no. 7, pp. 640–653, July 1993.

[48] D. J. Tyler and D. M. Durand, "Functionally selective peripheral nerve stimulation with a flat interface nerve electrode," *IEEE Transactions on Neural Systems and Rehabilitation Engineering*, vol. 10, no. 4, pp. 294–303, Dec 2002.

[49] J. Wells, C. Kao, K. Mariappan, J. Albea, E. D. Jansen, P. Konrad, and A. Mahadevan-Jansen, "Optical stimulation of neural tissue in vivo," *Optics Letters*, vol. 30, no. 5, pp. 504–506, Mar 2005. [Online]. Available: http://ol.osa.org/abstract.cfm?URI=ol-30-5-504

[50] M. G. Shapiro, K. Homma, S. Villarreal, C.-P. Richter, and F. Bezanilla, "Infrared light excites cells by changing their electrical capacitance," *Nature communications*, vol. 3, no. 736, 2012.

[51] "COMSOL multiphysics," COMSOL AB, Stockholm, Sweden, 2017. [Online]. Available: www.comsol.com

[52] J. W. Eaton, D. Bateman, S. Hauberg, and R. Wehbring, *GNU Octave version 4.0.0 manual: a high-level interactive language for numerical computations*, 2015. [Online]. Available: http://www.gnu.org/software/octave/doc/interpreter

[53] Python Software Foundation. Version 2.7.12. [Online]. Available: https:

//www.python.org

[54] C. A. Schneider, W. S. Rasband, and K. W. Eliceiri, "NIH image to ImageJ: 25 years of image analysis," *Nature methods*, vol. 9, no. 7, pp. 671–675, 2012, PMID:22930834.

[55] C. Gabriel and S. Gabriel, "Compilation of the dielectric properties of body tissues at RF and microwave frequencies," June 1996. [Online]. Available: http://niremf.ifac.cnr.it/docs/DIELECTRIC/Report.html#Param_Desc_of_Diel_Spect

[56] S. Gabriel. (1997) Compilation of the dielectric properties of body tissues at RF and microwave frequencies. Appendix C. [Online]. Available: http://niremf.ifac.cnr.it/docs/DIELECTRIC/AppendixC.html

[57] J. M. Barkmeyer and E. S. Luschei, "Quantitative analysis of the anatomy of the epineurium of the canine recurrent laryngeal nerve," *Journal of Anatomy*, vol. 196, no. 1, pp. 85–101, 2000.

[58] S. S. Burks, D. J. Levi, S. Hayes, and A. D. Levi, "Challenges in sciatic nerve repair: anatomical considerations," *Journal of Neurosurgery*, vol. 121, no. 1, pp. 210–218, 2014, pMID: 24724849. [Online]. Available: https://doi.org/10.3171/2014.2.JNS131667

[59] J. M. Bilbao and R. E. Schmidt, *Biopsy Diagnosis of Peripheral Neuropathy*, 01 2015.

[60] B. Kundalić, S. Ugrenović, I. Jovanović *et al.*, "Analysis of fascicular structure and connective tissue sheaths in sural nerve during aging," *Acta Facultatis Medicae Naissensis*, vol. 31, no. 2, pp. 113–120, 2004.

[61] F. Merli, B. Fuchs, J. R. Mosig, and A. K. Skrivervik, "The effect of insulating layers on the performance of implanted antennas," *IEEE Transactions on Antennas and Propagation*, vol. 59, no. 1, pp. 21–31, Jan 2011.

[62] M. Tømmer, K. G. Kjelgård, and T. S. Lande, "Body coupled wideband monopole antenna," pp. 1–5, Nov 2016.

[63] J.-P. Berenger, "A perfectly matched layer for the absorption of electromagnetic waves," *Journal of Computational Physics*, vol. 114, no. 2, pp. 185 – 200, 1994. [Online]. Available: http://www.sciencedirect.com/science/article/pii/S0021999184711594

[64] J. E. Mark, *Polymer Data Handbook*. Oxford University Press, 1999.

[65] P. Hasgall, F. Di Gennaro, C. Baumgartner *et al.* (2015, sept) IT'IS database for thermal and electromagnetic parameters of biological tissues. Version 3.0. [Online]. Available: www.itis.ethz.ch/database

[66] C. L. Brace, "Radiofrequency and microwave ablation of the liver, lung, kidney, and bone: What are the differences?" *Current Problems in Diagnostic Radiology*, vol. 38, no. 3, pp. 135–143. [Online]. Available: https://www.ncbi.nlm.nih.gov/pmc/articles/PMC2941203/

[67] R. Hansen, "Focal region characteristics of focused array antennas," *IEEE Transactions on Antennas and Propagation*, vol. 33, no. 12, pp. 1328–1337, Dec 1985.

[68] A. Buffi, P. Nepa, and G. Manara, "Design criteria for near-field-focused planar arrays," *IEEE Antennas and Propagation Magazine*, vol. 54, no. 1, pp. 40–50, Feb 2012.